Published in final edited form as:
Nat Neurosci. 2023 January ; 26(1): 64–78. doi:10.1038/s41593-022-01214-2.

Intracellular chloride regulation mediates local sleep pressure in the cortex

Hannah Alfonsa[1,*], **Richard J. Burman**[1], **Paul J. N. Brodersen**[1], **Sarah E. Newey**[1], **Kashif Mahfooz**[1], **Tomoko Yamagata**[2], **Marios C. Panayi**[3], **David M. Bannerman**[3], **Vladyslav V. Vyazovskiy**[2], **Colin J. Akerman**[1,*]

[1]Department of Pharmacology, University of Oxford; Mansfield Road, Oxford, OX1 3QT, UK

[2]Department of Physiology, Anatomy and Genetics, University of Oxford; Parks Road, Oxford OX1 3PT, UK

[3]Department of Experimental Psychology, University of Oxford; 15 Parks Road, Oxford, OX1 3AQ, UK

Abstract

Extended wakefulness is associated with reduced performance and the build-up of sleep pressure. In the cortex, this manifests as changes in network activity. These changes show local variation depending on the waking experience, and their underlying mechanisms represent targets for overcoming the effects of tiredness. Here we reveal a central role for intracellular chloride regulation, which sets the strength of postsynaptic inhibition via $GABA_A$ receptors in cortical pyramidal neurons. Wakefulness results in depolarizing shifts in the equilibrium potential for $GABA_A$ receptors, reflecting local activity-dependent processes during waking, and involving changes in chloride cotransporter activity. These changes underlie electrophysiological and behavioral markers of local sleep pressure within cortex — including the levels of slow-wave activity during non-rapid eye movement sleep — as well as low-frequency oscillatory activity and reduced performance levels in the sleep-deprived awake state. These findings identify chloride regulation as a crucial link between sleep–wake history, cortical activity and behavior.

*Corresponding authors: Hannah Alfonsa, hannah.alfonsa@pharm.ox.ac.uk, Colin J. Akerman, colin.akerman@pharm.ox.ac.uk.

Author contributions statement
HA and CJA conceptualized the project. HA and CJA designed the *in vitro* experiments. HA, CJA and VVV designed the *in vivo* electrophysiology experiments. HA, CJA, VVV, MCP and DMB designed the behavioral experiments. HA performed and analyzed the *in vitro* electrophysiology experiments. RJB performed *in vivo* gramicidin perforated patch recordings. HA and SEN performed the western blot experiments. HA performed and analyzed the *in vivo* electrophysiology experiments. KM performed the in utero electroporations. TY assisted with the optogenetics experiments. HA performed and analyzed the behavioral experiments. PB performed the neuronal network modelling and wrote the automated sleep scoring algorithm. HA and CJA wrote the manuscript with input from all authors.

Competing interests statement
The authors declare no competing interests.

Ethical approval
All experiments were performed in accordance with the United Kingdom Animal Scientific Procedures Act 1986 under personal and project licences granted by the United Kingdom Home Office. Approval was also provided by an Ethical Review Panel at the University of Oxford.

Europe PMC Funders Author Manuscripts

Europe PMC Funders Author Manuscripts

Introduction

An increase in sleep pressure (‘need to sleep’) is associated with a reduction in cognitive performance and changes in cortical activity that can be detected during the sleep-deprived state and during sleep[1–4]. Whilst significant progress has been made in understanding the changes that accompany waking and sleeping[5–8], we still lack an appreciation of the mechanisms that translate an animal’s sleep–wake history into the altered network activities and behaviors associated with tiredness. Identifying the underlying mechanisms should provide a functional account of the changes in cortical activity that occur with wakefulness and generate opportunities to restore performance levels when we are tired.

One marker of sleep pressure is the level of slow-wave activity (SWA) recorded in the cortical electroencephalogram (EEG; spectral power between 0.5 to 4 Hz) during non-rapid eye movement (NREM) sleep[2,4,9–11]. Levels of SWA increase as a function of preceding wakefulness and lessen as a function of sleep. SWA involves the low-frequency switching between periods of action-potential spiking activity amongst cortical neurons (‘ON periods’, associated with cortical up states) and periods of neuronal silence (‘OFF periods’, associated with cortical down states)[9]. The oscillations underlying SWA reflect thalamocortical interactions[12] and the increased levels of SWA that occur under conditions of high sleep pressure are associated with greater and more synchronous spiking activity amongst populations of cortical neurons[9,13].

Markers of sleep pressure also vary temporally and spatially across cortex, in a manner that reflects the duration and task-dependent demands of the preceding wake period[2,4,9,11,14]. Cortical regions that are most active during waking tend to show the highest levels of NREM SWA, supporting the idea that sleep pressure is locally regulated within cortex[10,11,14]. In a related manner, wakefulness leads to increases in low-frequency cortical oscillations in the sleep-deprived awake EEG, which show spectral overlap with SWA[1,3,14], and can be considered a cortical marker of high sleep pressure in the awake state. Referred to as ‘local sleep’ in the awake brain, this phenomenon is also associated with preceding task-dependent demands and has been proposed to contribute to the drops in cortical function and behavioural performance when we are tired[1,3,15].

At a cellular level, important advances have come from investigating the activity-dependent changes in neuronal properties that underlie sleep-wake dynamics[16,17]. However, there has been surprisingly little focus on the key ions that determine neuronal excitability. Studies in circadian systems have revealed that pacemaker neurons of the suprachiasmatic nucleus exhibit diurnal variations in their transmembrane gradients for chloride (Cl^-), which affects inhibitory synaptic transmission mediated by the gamma-aminobutyric acid type A receptor ($GABA_AR$)[18,19]. As $GABA_ARs$ are primarily permeable to Cl^-, the equilibrium potential for the $GABA_AR$ ($EGABA_A$) is dependent on the transmembrane Cl^- gradients that determine a neuron’s equilibrium potential for Cl^- (ECl^-). $EGABA_A$ is determined by Cl^- cotransporter proteins and typically resides close to a neuron’s resting membrane potential[20–22]. In addition to inhibitory shunting effects, more-negative $EGABA_A$ values favour stronger synaptic inhibition through hyperpolarization of the post-synaptic membrane, whereas more-positive $EGABA_A$ values favour weaker synaptic inhibition and can depolarize the

membrane. Indeed, these scenarios have been observed in mature cortical neurons, but have not been examined in the context of sleep-wake dynamics[20,22,23].

Here we demonstrate that $EGABA_A$ in cortex translates sleep–wake history into changes in network activity and behavior that are associated with sleep pressure. *In vitro* and awake *in vivo* recordings from mice reveal that $EGABA_A$ in cortical pyramidal neurons reflects the animal's sleep–wake history, becoming more depolarized following periods of wakefulness. These effects involve changes to Cl^- cotransporters, are activity-dependent, and show regulation at a local level. We show that these changes in $EGABA_A$ contribute to markers of local sleep pressure within cortex. Specifically, wake-dependent depolarizing shifts in $EGABA_A$ were found to influence levels of SWA during NREM sleep by enhancing neuronal recruitment during cortical ON periods, to promote low-frequency oscillatory activity when sleep pressure is high in awake cortex, and to underlie task-specific drops in performance levels in the sleep-deprived awake state.

Results

$EGABA_A$ varies diurnally in cortical pyramidal neurons

We assessed $EGABA_A$ in cortical pyramidal neurons at different time points during the 24-hour light–dark cycle. These time points were associated with different sleep–wake histories, as confirmed by continuous EEG and electromyography (EMG) recordings (Fig. 1a). As expected, mice spent a high proportion of time asleep and awake during the light and dark period, respectively (Fig. 1b). $EGABA_A$ measurements were performed in acute somatosensory cortical brain slices prepared from mice either 3 hours after light onset (i.e. Zeitgeber time 3, ZT3), which is associated with recent sleep, or 3 hours after dark onset (ZT15), which is associated with recent waking.

Pyramidal neurons in layer 5 (L5) were targeted in primary somatosensory cortex (S1) using the gramicidin perforated patch recording technique, which avoids disruption of the neuron's native $[Cl^-]_i$ (Fig. 1c). Recordings in current clamp configuration (I=0 mode) revealed that ZT3 neurons showed predominantly hyperpolarizing responses to brief puffs of GABA at the neuron's soma (Fig. 1d). By contrast, a high proportion of ZT15 neurons exhibited depolarizing $GABA_AR$ responses, such that the distribution of responses was significantly different between the two recording times (Fig. 1d). The depolarizing $GABA_AR$ responses rarely initiated action potentials (95% no action potential; n=20/21 neurons), consistent with reports of depolarizing $GABA_AR$ responses in mature cortical neurons, where the equilibrium potential for the $GABA_AR$ ($EGABA_A$) is more depolarized than the resting membrane potential, but below the threshold for action potentials[20,22,23]. No difference was observed in the resting membrane potential (ZT3: -77.71 ± 5.92 mV and ZT15: -76.22 ± 6.96 mV; p=0.49, unpaired t-test; t=0.7; df=38) or membrane resistance (ZT3: 170.8 ± 67.67 MΩ and ZT15: 167.02 ± 44.28 MΩ; p=0.48, unpaired t-test; t=0.72; df=36) between the two recording times.

To support these observations, we performed direct measurements of $EGABA_A$ in voltage clamp mode, which involves measuring the current passing through activated $GABA_ARs$ at different membrane potentials and provides an estimate of $EGABA_A$ that is independent

of the $GABA_AR$ conductance (Fig. 1e and Supplementary Fig. 1). Mice at ZT3 exhibited hyperpolarized $EGABA_A$ values, consistent with a hyperpolarized ECl^- and low $[Cl^-]_i$. By contrast, mice at ZT15 exhibited more depolarized $EGABA_A$ values, consistent with a more depolarized ECl^- and higher $[Cl^-]_i$ (Fig. 1f and Extended Data Fig. 1). Consistent with the current clamp recordings, $GABA_AR$ driving forces were more depolarizing at ZT15 than at ZT3 (Extended Data Fig. 2a). The same difference was observed in the presence of tetrodotoxin (TTX) to prevent action potentials in the brain slices, with neurons at ZT3 exhibiting more hyperpolarized $EGABA_A$ values when compared to neurons at ZT15 (Fig. 1g and Extended Data Fig. 1), indicating that these observations are independent of potential differences in network activity. Experiments on L2/3 pyramidal neurons in auditory cortex showed similar differences between ZT3 and ZT15, indicating that the diurnal difference in $EGABA_A$ is not unique to a cortical layer or region (Fig. 1h and Extended Data Fig. 1). Finally, control experiments were conducted to rule out the potential contribution of GABA receptors during the recordings, and to assess the changes via an alternative Cl^--permeable channel. These experiments used the activation of the glycine receptor, which is also primarily permeable to Cl^-, and blocked $GABA_ARs$ and $GABA_BRs$ with selective antagonists (Extended Data Fig. 1d,e). Again, these recordings revealed that slices prepared from mice at ZT3 exhibited more hyperpolarized EGlycine values than slices prepared from mice at ZT15. Across all of the experimental conditions, the mean difference in $EGABA_A$/EGlycine between ZT3 and ZT15 was 11.1 mV, which is equivalent to an estimated shift in $[Cl^-]_i$ of approximately 4 mM (Extended Data Fig. 1f).

$[Cl^-]_i$ is determined by cotransporter proteins in the cell membrane and the relative activity of oppositely directed cotransporters can generate temporal and spatial differences in a neuron's $EGABA_A$[22]. To investigate the mechanism underlying cortical $EGABA_A$ dynamics across the 24-hour light-dark cycle, we measured the contribution of the potassium-chloride exporter KCC2 and the sodium-potassium-chloride importer NKCC1, by blocking them with VU0463271 ('VU') and bumetanide, respectively. Consistent with evidence that KCC2 is a regulator of $[Cl^-]_i$ in cortex[24], VU caused a robust depolarizing shift in $EGABA_A$ in cortical pyramidal neurons at both ZT3 and ZT15 (Fig. 1i; ZT3: 9.39 ± 3.27 mV, p=0.0009, one sample t-test; t=7.04; df=5; ZT15: 12.37 ± 6.2 mV; p=0.011, one sample t-test; t=4.46; df=4). By contrast, blocking NKCC1 with bumetanide had no effect at ZT3 (Fig. 1j; ZT3: 1.19 ± 1.63 mV; p=0.079, one sample t-test; t=2.057; df=7), but caused a significant hyperpolarizing shift in $EGABA_A$ when applied at ZT15 (Fig. 1j; ZT15: -2.54 ± 2.49 mV, p=0.024, one sample t-test; t=2.881; df=7), consistent with a greater contribution of NKCC1 to $EGABA_A$ at ZT15 (Fig. 1j). These data suggest that the contribution of NKCC1 to $EGABA_A$ changes across the 24-hour cycle, whereas KCC2's contribution to $EGABA_A$ does not. Thus, cortical pyramidal neurons exhibit diurnal variations in $EGABA_A$, which are consistent with observed changes in $[Cl^-]_i$[25], and are associated with changes in chloride cotransporter activity.

Preceding sleep–wake history determines $EGABA_A$ in cortex

Diurnal variations in $EGABA_A$ have previously been shown to modulate $GABA_AR$ signalling within the principal circadian pacemaker of the mammalian brain, the SCN[18,19]. In addition to circadian phase however, different times of day correspond to different sleep–

wake histories in an animal that is entrained to the light-dark cycle. We therefore used a sleep deprivation (SD) paradigm to test whether the diurnal changes in cortical $EGABA_A$ reflect the animal's preceding sleep–wake history. If $EGABA_A$ reflects circadian phase, mice experiencing SD during the first 3h of the light period ('ZT3-SD') should be similar to the control ZT3 condition. However, if cortical $EGABA_A$ levels are determined by preceding sleep-wake history, ZT3-SD should be similar to the ZT15 condition, when animals had typically been awake for several hours and built up spontaneous sleep pressure (Extended Data Fig. 3a). EEG recordings confirmed that the sleep-deprived mice were successfully kept awake during the first 3h of the light period (Fig. 2a) and showed the hallmark of high sleep pressure in the form of increased cortical SWA during NREM sleep (Fig. 2b).

We prepared acute cortical brain slices from ZT3-SD mice and performed gramicidin perforated patch recordings. Current clamp recordings from ZT3-SD mice revealed depolarizing responses to brief puffs of GABA at the neuron's soma (Fig. 2c) and represented a significant increase in the proportion of depolarizing $GABA_AR$ responses in the high sleep-pressure condition of ZT3-SD, compared to the low sleep-pressure condition of ZT3 (Fig. 2c). Again, the depolarizing $GABA_AR$ responses in ZT3-SD mice rarely initiated action potentials (77% no action potential; n=10/13 neurons) and no difference was observed in resting membrane potential (ZT3: -77.71 ± 5.92 mV and ZT3-SD: -75.6 ± 24.69 mV; p=0.498, unpaired t-test; t=0.6608; df=24) or membrane resistance (ZT3: 170.8 ± 67.67 MΩ and ZT3-SD: 162.84 ± 71.11 MΩ; p=0.77, unpaired t-test; t=0.3, df=25) across condition. These observations were corroborated by measurements of $EGABA_A$, which was more depolarized in the ZT3-SD mice than in the ZT3 mice (Fig. 2d and Extended Data Fig. 2b).

To establish if sleep–wake history modulates $GABA_AR$ signalling in the intact brain, we performed *in vivo* gramicidin perforated recordings in awake mice. These recordings used light-activation of channelrhodopsin-2 (ChR2) expressing interneurons to assess the effect of post-synaptic $GABA_AR$ activation in L2/3 pyramidal neurons from ZT3 control mice and ZT3-SD mice (Fig. 2e). Current clamp recordings revealed significantly more depolarizing responses to synaptic $GABA_AR$ activation in the ZT3-SD mice compared to control mice at ZT3 (Fig. 2f). There was no difference in the resting membrane potential (Fig. 2f) or membrane resistance (ZT3: 136.22 ± 37.52 MΩ and ZT3-SD: 126.85 ± 26.44 MΩ; p=0.56, unpaired t-test; t=0.6; df=16). These awake *in vivo* recordings that preserve transmembrane Cl^- gradients support the conclusion that sleep–wake history determines the polarity of $GABA_AR$ signalling. The more depolarized $EGABA_A$ following SD was also associated with increased NKCC1 activity, as the bumetanide-induced shift in $EGABA_A$ measured *in vitro* was larger following SD (Fig. 2g). Additionally, western blot experiments revealed an increase in total NKCC1 protein levels in somatosensory cortex (Fig. 2h), which was supported by immunostaining experiments in L5 neurons of S1 following SD (Extended Data Fig. 4). The ZT3-SD condition was therefore more similar to the ZT15 condition than to the ZT3 condition, suggesting that the observed changes in $EGABA_A$ reflect preceding sleep–wake history, with more depolarized $EGABA_A$ values being associated with recent periods of wakefulness.

The effects of wakefulness in cortex have been shown to reflect task-dependent demands and local activity-dependent processes during the preceding wake period[2,4,11,14]. To assess whether increases in $EGABA_A$ reflect activity-dependent processes during the preceding wake period, we used an established whisker-trimming paradigm[11] to disrupt somatosensory-evoked cortical activity. Whiskers were trimmed unilaterally at ZT3, when $EGABA_A$ is normally hyperpolarized. Mice were then subjected to 3 hours of SD so that they would remain awake and able to use their whiskers on the intact side, but not on the trimmed side (Fig. 2i). This protocol resulted in a shift towards depolarizing $GABA_AR$ responses in L5 pyramidal neurons in the hemisphere contralateral to the intact whiskers, confirming our earlier observation that SD induces depolarizing shifts in $EGABA_A$ (Fig. 2j). This was not associated with a change in resting membrane potential (intact: -77.34 ± 5.23 mV and trimmed: -75.03 ± 1.71 mV; p=0.27; unpaired t-test with Welch correction; t=1.19; df=8) or membrane resistance (intact: 197.9 ± 104.38 MΩ and trimmed: 186.66 ± 69.75 MΩ; p=0.8, unpaired t-test; t=0.25; df=14). By contrast, neurons contralateral to the trimmed whiskers and recorded in the same brain slices continued to exhibit hyperpolarizing $GABA_AR$ responses, displaying more hyperpolarized $EGABA_A$ values and more hyperpolarizing $GABA_AR$ driving forces (Fig. 2j,k and Extended Data Fig. 2c). These data suggest that cortical $EGABA_A$ reflects activity-dependent processes during preceding wake periods and can be regulated at a local level, as has been shown for markers of sleep pressure in cortex[10,11,14].

$[Cl^-]_i$ regulation determines the level of local NREM SWA

Our findings so far indicate that when sleep pressure increases as a result of wakefulness, cortical neurons exhibit more depolarized $EGABA_A$ values, due in part to increased NKCC1 activity. Given the central role for synaptic inhibition in controlling network activity and function, we tested whether the changes in $EGABA_A$ contribute to markers of sleep pressure in cortex. The level of cortical SWA observed during NREM sleep is widely considered a key marker of sleep pressure[2,4,9–11]. If wakefulness-associated depolarizing shifts in $EGABA_A$ determine the level of cortical SWA, our prediction was that lowering $[Cl^-]_i$ would have its greatest impact when sleep pressure is high, at the beginning of the light period. To test this, we performed *in vivo* recordings in freely moving mice that had been implanted with a local field potential (LFP) electrode coupled with an infusion cannula, and targeted to L5 of S1 (Fig. 3a) for continuous LFP recordings. Antagonists of Cl^- cotransporter proteins were infused locally into S1 at different time points during the light period, which are associated with different levels of SWA (Fig. 3b; Extended Data Fig. 3b).

Bumetanide infusion at the beginning of the light period, when SWA is highest, caused pronounced reductions in the level of SWA (Fig. 3c,d). These effects were only evident in the local S1 LFP signal and not in the global frontal EEG (Fig. 3d, Extended Data Fig. 5 and 6), consistent with the idea that $[Cl^-]_i$ regulation can mediate regional differences in SWA[10]. By contrast, bumetanide infusion 2-3 hours after light onset, when sleep pressure and SWA levels have reduced as a result of natural sleep (Extended Data Fig. 2b), did not affect levels of SWA (Fig. 3e,f, Extended Data Fig. 5 and 6), whereas blocking KCC2 with VU at this later time point to increase $[Cl^-]_i$, did increase the level of local SWA (Fig. 3g,h, Extended Data Fig. 5 and 6). These data support the idea that changes in $EGABA_A$ provide a link

between an animal's sleep-wake history and the level of NREM SWA observed in cortex, which is a marker of sleep pressure.

Depolarized $EGABA_A$ boosts SWA via neuronal recruitment

Increases in the level of SWA with high sleep pressure are thought to result from greater and more synchronous spiking activity amongst populations of cortical neurons during ON periods[9]. As ON periods involve elevated excitatory and inhibitory synaptic activity[26,27], we hypothesized that neurons with depolarized $EGABA_A$ would be more likely to be recruited to spike during ON periods because their weaker synaptic inhibition would enable greater summation of excitatory inputs[28]. To test this, we generated brain slices from animals with different sleep– wake histories (ZT3 versus ZT15) and used cell-attached recordings to monitor L5 pyramidal neuron spiking in response to the stimulation of two independent input pathways from L2/3. The cell-attached configuration ensured that transmembrane Cl^- gradients remained intact and spike times were consistent with the recruitment of monosynaptic excitatory and feedforward inhibitory inputs[28] (Fig. 4a,b). Stimulus intensity was set such that the L5 neuron spiked on approximately half of the trials when the input pathways were stimulated simultaneously. As the delay between the two input pathways was increased, the probability of spiking decreased, consistent with previous work showing that feedforward synaptic inhibition determines a neuron's integration window[28]. Neurons at ZT15, which exhibit more depolarized $EGABA_A$ values, showed broader synaptic integration windows than neurons at ZT3 (Fig. 4b-d). Furthermore, reducing $[Cl^-]_i$ in ZT15 neurons, by infusing bumetanide, narrowed the integration window for spiking, whereas increasing $[Cl^-]_i$ in ZT3 neurons, by blocking KCC2 with VU, broadened the integration window (Fig. 4b-d). To complement these recordings, we also generated a simple network model that enabled us to selectively vary $EGABA_A$ in a population of excitatory neurons, whilst maintaining all other parameters (Fig. 4e; Methods). Network simulations with more depolarized $EGABA_A$ values showed greater recruitment of spiking activity during simulated ON periods (Fig. 4f,g), which was most pronounced when ON-OFF transitions occurred at lower frequencies (≤6 Hz; Fig. 4h). Therefore, through their effects on synaptic inhibition, depolarized $EGABA_A$ values resulting from preceding wakefulness can determine how easily a cortical neuron is recruited to spike, such as occurs during ON periods of SWA.

To test the contribution of $EGABA_A$ to SWA in the intact brain, we used an *in vivo* optogenetic strategy to control $EGABA_A$ in a population of cortical neurons in freely moving mice (Fig. 5a). Previous work has established that the light-activated Cl^- pump, halorhodopsin (eNpHR3.0), can be used to generate physiologically-relevant depolarizing shifts in $EGABA_A$ by causing transient increases in $[Cl^-]_i$[29,30]. Virally-delivered halorhodopsin was expressed in pyramidal neurons of S1 and a tetrode coupled with fibre optic was implanted to monitor and manipulate nearby neurons. $[Cl^-]_i$ was increased optically during periods of NREM sleep at ZT3, when sleep pressure is low and $EGABA_A$ is normally hyperpolarizing. The halorhodopsin-mediated increases in $[Cl^-]_i$ occur rapidly during light-activation and persist for tens of seconds after the light-activation has stopped[29,30], which provides sufficient time to compare electrophysiological signals under different levels of $[Cl^-]_i$ within the same neuron (Fig. 5a). LFP and multiunit activity were

therefore compared immediately before and after halorhodopsin activation, when levels of $[Cl^-]_i$ in the opsin-expressing neurons would be low and high, respectively (Fig. 5a-b).

Optically elevating $[Cl^-]_i$ in the halorhodopsin-expressing pyramidal neurons was associated with a pronounced increase in LFP spectral power in the lower frequency range (0.5 to 6 Hz; Fig. 5b,c). This effect recovered with a time constant of 12.7 ± 1.5 s (Extended Data Fig. 7a,c,d), consistent with the recovery of $EGABA_A$ by endogenous Cl^- cotransporters following a halorhodopsin-induced increase in $[Cl^-]_i$[29,30]. These effects were not observed with the light-activated outward proton pump, archaerhodopsin, which provided a control for membrane potential hyperpolarization without affecting $[Cl^-]_i$ (Fig. 5c and Extended Data Fig. 7b,e,f). To further analyse the neuronal recruitment into population ON and OFF periods, the timing of multiunit activity relative to slow waves was analysed before and after opsin activation. Phase plots of spike-time histograms showed that halorhodopsin-mediated increases in $[Cl^-]_i$ produced an increase in spiking activity during ON periods, which was not evident following archaerhodopsin activation (Fig. 5d and Extended Data Fig. 7g-l). Thus, selectively elevating $[Cl^-]_i$ in excitatory cortical neurons is sufficient to increase their recruitment during ON periods and boost local SWA. $EGABA_A$ therefore provides a mechanistic link between sleep-wake history and the spatial and temporal regulation of cortical SWA, which is a marker of sleep pressure.

$[Cl^-]_i$ regulation underlies markers of high sleep pressure

Sleep deprivation (SD) produces electrophysiological markers of high sleep pressure, which can be detected both in the sleep-deprived awake state and when an animal goes to sleep. For example, low-frequency cortical oscillations that show spectral overlap with SWA, are increased in the sleep-deprived awake EEG[1,3,15]. Low-frequency oscillations in the awake EEG can also reflect task-dependent demands during the preceding wake period and have been viewed as evidence of 'local sleep' in the awake brain[1,3,15,31]. To examine whether cortical $[Cl^-]_i$ regulation underlies this marker of local sleep pressure in cortex, we first confirmed that the awake S1 LFP and frontal EEG show increased power at low frequencies (2 to 6 Hz), when mice experienced a 3h SD protocol at the beginning of light onset (Fig. 6a-c) that leads to depolarizing $EGABA_A$ (Fig. 2d). If depolarizing $EGABA_A$ contributes to the low-frequency oscillations in the sleep-deprived awake state, we predicted that blocking chloride transporters during the SD protocol would affect these signals. In line with this prediction, infusing bumetanide into S1 reduced the local low-frequency oscillatory activity in the sleep-deprived state, without affecting the global EEG (Fig. 6c, Extended Data Fig. 8a), whereas raising $[Cl^-]_i$ further with local VU application augmented low-frequency oscillatory activity in the LFP, but not in the global EEG (Fig. 6c, Extended Data Fig. 8a).

To relate the level of low-frequency oscillations to activity-dependent processes during the period of SD, we combined the whisker-trimming paradigm (as in Fig. 2) with LFP and EEG measurements (Fig. 6d). In response to SD, the build-up of awake low-frequency oscillations was reduced in the hemisphere contralateral to the trimmed whiskers, but was unaffected in the global EEG (Fig. 6e, Extended Data Fig. 8b). Under these conditions, the levels of low-frequency oscillations in contralateral S1 could be rescued by local infusion of VU (Fig. 6e, Extended Data Fig. 8b). These observations support the idea that local, activity-

dependent depolarizing shifts in $EGABA_A$ underlie increases in low-frequency oscillatory cortical activity that are associated with high sleep pressure in the sleep-deprived awake state.

High sleep pressure following SD is also associated with an increase in SWA when the animal goes to sleep[4,9,10]. We therefore monitored the S1 LFP and frontal EEG in the same SD animals as they entered NREM sleep (Fig. 7a). Lowering $[Cl^-]_i$ by infusing bumetanide into S1 at the beginning of SD led to a reduction in local SWA during NREM sleep (Fig. 7b,c, Extended Data Fig. 9), consistent with a reduction in this marker of local sleep pressure, whereas raising $[Cl^-]_i$ by VU infusion led to a further enhancement in local SWA during NREM (Fig. 7b,c, Extended Data Fig. 9). Finally, by combining the whisker-trimming and SD paradigms, we found that whisker-trimming prevented the normal increase in local SWA as the animals entered NREM sleep, and that high levels of SWA in S1 could be rescued by raising $[Cl^-]_i$ through local VU infusion (Extended Data Fig. 10). Taken together, these data support the conclusion that $[Cl^-]_i$ regulation underlies electrophysiological markers of high sleep pressure observed with sleep deprivation.

$[Cl^-]_i$ regulation affects sleep-deprived performance levels

Like humans, mice show reduced cognitive and behavioral performance levels when sleep pressure is high[1,32,33]. Indeed, such decreases in performance have been linked to increases in low-frequency cortical oscillations in the sleep-deprived awake EEG[1,3,15]. We considered the possibility that altering $EGABA_A$ could reverse the drops in performance associated with sleep deprivation. To test this, we investigated the impact of cortical $[Cl^-]_i$ on performance on novel-object recognition (NOR) tasks, which involve relevant sensory systems[34,35]. We compared performance levels in sleep-deprived animals that had experienced 3 hours of SD at the beginning of light onset to rested animals that were not sleep-deprived and were allowed to sleep during the equivalent 3-hour period (Fig. 8a). We manipulated $[Cl^-]_i$ in S1 and compared performance across odor-based (see Methods) and tactile-based (Fig. 8b) versions of the task.

First, we confirmed previous observations that SD results in decreased performance levels[32,33], here resulting in lower novelty preference on both the tactile NOR task (Fig. 8c) and the odor-based NOR task (Fig. 8f). If elevated $[Cl^-]_i$ and the associated increase in low-frequency cortical oscillations contribute to these decreased performance levels, reducing $[Cl^-]_i$ in S1 would be expected to improve performance on the tactile task but not on the odor task. In line with this prediction, reducing $[Cl^-]_i$ by local infusion of bumetanide into S1 of sleep-deprived animals resulted in increased NOR performance on the tactile task (Fig. 8d). This manipulation in S1 did not influence performance on the odor task, consistent with a local rather than global effect on cortex (Fig. 8g). Finally, to test the idea that an increase in cortical $[Cl^-]_i$ is sufficient to compromise performance, we conducted experiments in animals that had not been sleep-deprived and had been allowed to rest normally. Increasing $[Cl^-]_i$ by local infusion of VU into S1 caused rested animals to show reduced NOR performance on the tactile task (Fig. 8e). Again, this manipulation did not influence performance on the odor task, consistent with a local effect on cortex (Fig. 8h).

Taken together, these results support the conclusion that cortical $EGABA_A$ contributes to performance levels observed in the sleep-deprived awake state.

Discussion

Our findings (summarised in Supplementary Fig. 2) reveal that a cortical pyramidal neuron's synaptic $EGABA_A$ reflects the animal's sleep–wake history, exhibiting more depolarized values after periods of wakefulness. The depolarizing shifts in $EGABA_A$ show activity-dependent differences across cortex, consistent with evidence that sleep pressure exhibits use-dependent local variation[1–3,10,11,14,15]. We then show that these wake-dependent changes in $EGABA_A$ contribute to electrophysiological and behavioral changes associated with the levels of sleep pressure within the cortex. Firstly, we implicate the $EGABA_A$ changes in the level of NREM SWA, a neural correlate of sleep pressure measured during sleep[4,9]. Wake-dependent depolarizing shifts in $EGABA_A$ weaken postsynaptic inhibition, raising spiking levels and synchrony amongst nearby neurons, which underlies elevated SWA when sleep pressure is high[9]. This was no longer the case when sleep pressure and NREM SWA levels reduce following a period of sleep. Our data also implicate the $EGABA_A$ changes in markers of sleep pressure in the sleep-deprived awake state, which include low-frequency oscillatory activity in cortex and drops in behavioral performance levels. Reducing $[Cl^-]_i$ to hyperpolarizing $EGABA_A$ in sleep-deprived animals was sufficient to attenuate local low-frequency cortical oscillations and restore performance levels in a task-specific manner.

Although laboratory mice have polyphasic sleep patterns, with most of their sleep taking place during the light period, mice exhibit neurophysiological changes associated with sleep pressure that are shared across mammalian species, including humans. This involves increases in the levels of NREM SWA after periods of extended wakefulness, the fact that sleep dissipates increased SWA, plus the fact that low-frequency oscillations are observed in the tired awake state, and that markers of sleep pressure exhibit use-dependency and local variation[1–4,9–11,14,15,36]. Our gramicidin recordings at ZT3 and ZT15 established that cortical pyramidal neurons show diurnal variations in $EGABA_A$, with more hyperpolarizing $GABA_AR$ responses and $EGABA_A$ values observed at ZT3, and more depolarizing $GABA_AR$ responses and $EGABA_A$ values at ZT15. This pattern was confirmed in multiple cortical areas, cortical layers, and in both juvenile and adult cortex. These data are consistent with evidence from anaesthetized mice of diurnal variations in somatic chloride concentration, with higher values in the period corresponding to waking[25]. However, diurnal variation does not necessarily reflect circadian regulation, due to the potential contribution of sleep-wake history. Therefore, we also investigated the effects of sleep-wake history using a sleep-deprivation paradigm that achieves a more physiologically normal arousal state than other paradigms[37]. Importantly, this protocol controls for both the light-dark cycle and circadian processes, enabling us to directly compare animals at the same point in the circadian cycle, but with different sleep-wake histories. Under these conditions, awake *in vivo* gramicidin recordings and *in vitro* recordings established that $EGABA_A$, and the polarity of postsynaptic $GABA_AR$ signalling in the awake cortex, reflect the animal's sleep-wake history.

Although the waking experience may matter[38] and sleep deprivation may, in some cases, differ from spontaneous wakefulness[37,39], multiple aspects of our study support the conclusion that $EGABA_A$ reflects sleep-wake history. Firstly, the direction of $EGABA_A$ change and the underlying mechanism were similar between spontaneous wakefulness and sleep deprivation, with both showing less hyperpolarized $EGABA_A$ values and greater activity of the NKCC1 cotransporter. Secondly, reducing $EGABA_A$ by local infusion of bumetanide resulted in reduced local SWA in animals that have high sleep pressure due to both spontaneous wakefulness and sleep deprivation. And finally, causing acute depolarizing shifts in $EGABA_A$, either pharmacologically or optogenetically, elicited comparable effects on markers of sleep pressure associated with both spontaneous wakefulness and sleep deprivation.

$EGABA_A$ is determined by a neuron's transmembrane chloride fluxes, which reflect the activity of multiple channel and transporter proteins in the membrane[40]. We investigated two major contributors, the cotransporters KCC2 and NKCC1[20–22]. Our studies indicated that the contribution of the Cl^- importer NKCC1 to $EGABA_A$ in L5 pyramidal neurons is higher when sleep pressure is high, either following spontaneous wakefulness or SD, and this was supported by evidence that NKCC1 is upregulated at the molecular level. The fact that NKCC1's contribution to $EGABA_A$ was only detected following periods of wakefulness in the mouse, which typically correlate with our night time, may have contributed to this cotransporter being underappreciated in the mature cortex. Meanwhile, our electrophysiological studies indicated that the Cl^- exporter KCC2 makes a similar, strong hyperpolarizing contribution to $EGABA_A$ at both ZT3 and ZT15, when measured at the soma of L5 pyramidal neurons. These data do not exclude potential changes in KCC2 activity however, which may be detectable under different recording conditions, or in other neuronal populations and cellular compartments[40]. Similarly, our experiments did not consider alternative chloride fluxes, which could contribute to the sleep-wake related changes in $EGABA_A$ that we observe. Recent evidence supports diurnal variations in the phosphorylation status of NKCC1 and KCC2[25], and a proteomics screen to reveal sleep-wake related phosphopeptides and their kinases from neurons in mouse forebrain, identified NKCC1 (Slc12a2) and WNK1 kinase[6] - a kinase that regulates NKCC1 and KCC2[22]. These observations highlight that there may be multiple chloride fluxes involved, as well as mechanisms upstream that translate the animal's experience into the cellular changes. This is a rich area for future investigation, given that chloride homeostasis can be modulated by a variety of mechanisms, ranging from local activity-dependent signals, to more widespread signalling systems, such as hormones[22,41,42].

The local and bidirectional modulation of $[Cl^-]_i$ enabled us to investigate properties of local sleep pressure within the cortex without eliciting global effects on the animal. Pharmacological experiments enabled us to test whether wake-dependent increases in $[Cl^-]_i$ contribute directly to markers of sleep pressure. For example, in the case of SWA levels during NREM sleep, local bumetanide infusion resulted in a reduction in local SWA when sleep pressure was high, whereas the same manipulation had no effect when sleep had reduced the levels of sleep pressure and NKCC1 activity. Conversely, VU infusion was able to rescue cortical markers of sleep pressure in whisker-deprived animals that exhibit reduced local sleep pressure in somatosensory cortex. Within the framework of global sleep

homeostasis, the level and dynamics of sleep pressure accumulation is thought to affect the properties of subsequent sleep[4,9,13]. This idea is consistent with the experiments in which bumetanide infusion during a period of SD resulted in lower levels of local SWA when the animal entered NREM sleep.

We therefore identify $EGABA_A$ as a key parameter by which cortical neurons translate sleep-wake history into ongoing changes in cortical network activity and function. As $EGABA_A$ determines how a neuron responds to its synaptic inputs, this can be considered a cell-specific mechanism, well-suited to mediating local changes. This is in line with the growing appreciation that sleep homeostasis involves a set of distributed processes, involving cortical and subcortical circuits, acting both locally and globally[1,10,11,13–15,41,43,44]. Within cortex, the interplay between inhibitory and excitatory synaptic inputs means that $EGABA_A$ changes are likely to interact with other processes that contribute to sleep-wake dynamics. For instance, depolarized $EGABA_A$ would be predicted to enhance the recruitment of voltage-gated potassium channels that contribute to oscillatory activity associated with sleep[45,46]. $EGABA_A$ also links to evidence that glutamatergic synaptic strength varies with sleep-wake history[16,17,47–49], as synaptic inhibition gates the induction of glutamatergic synaptic plasticity[50,51]. There are also parallels with evidence from the suprachiasmatic nucleus of the hypothalamus, where diurnal changes in $EGABA_A$ have been linked to circadian processes[18,19]. Indeed, future work could examine whether circadian mechanisms also influence $EGABA_A$ in cortex, perhaps by studying animal models that have altered circadian rhythms[52,53]. Similarly, one could investigate whether sleep-wake history contributes to $EGABA_A$ changes that have been observed in the brain circuits that regulate circadian rhythms.

Finally, our results provide a new context for understanding sleep disturbances associated with conditions such as epilepsy, autism, and schizophrenia, in which altered intracellular chloride regulation has been reported in cortical regions[54,55]. This raises the question of whether changes in $EGABA_A$ represent a primary pathology or a secondary result of changes in sleep-wake patterns. Either way, the co-occurrence of altered $[Cl^-]_i$ and sleep disturbances provides further motivation to target chloride regulatory mechanisms and, by accounting for sleep-wake history, improve therapeutic effects.

Methods

Animal husbandry and sleep deprivation

Unless stated, experiments were performed on male C57BL/6 wild-type mice purchased from Charles River. Animals were maintained under a 12-h:12-h light-dark (LD) cycle. Ambient room temperature was maintained at 22 ± 2°C and humidity at 50 ± 20%. Animals were aged 4-12 weeks and animal numbers are provided in the figure legends for each experiment. Animals were maintained under a 12-h:12-h light-dark (LD) cycle. Animals used for sleep deprivation (SD) protocols were singly housed and pre-exposed to novel objects in the days preceding the experiment, to encourage exploratory behavior. The timing of SD is stated at the relevant points in the manuscript (Fig. 2a, 2i, 6a, 6d, 7a, 8a). The SD protocol consisted of delivering novel objects under continuous observation by an experimenter. Once an animal had stopped exploring an object, a new object was presented.

This protocol resulted in the animal being awake for 99.2±1.32% (mean ± stdev) of the SD period.

Acute brain slices

Acute cortical brain slices were prepared for electrophysiological recordings from 4-12 week old mice at a defined zeitgeber time (ZT). The time of sacrifice is stated at the relevant points in the manuscript (Fig. 1b, 2a, 2i, 4b). Animals from the same litter were randomly assigned to the different ZT conditions. To prepare acute slices, animals were collected, and immediately sacrificed by neck dislocation and decapitation. Coronal 350 μm slices were cut using a vibrating microtome (Microm HM650V) in a pre-chilled cutting solution containing (in mM): 65 Sucrose, 85 NaCl, 2.5 KCl, 1.25 NaH_2PO_4, 7 $MgCl_2$, 0.5 $CaCl_2$, 25 $NaHCO_3$ and 10 glucose, pH 7.2–7.4 and bubbled with carbogen (95% O_2/5% CO_2). Slices were then incubated for at least 1 h in a storage chamber containing artificial cerebrospinal fluid (aCSF; in mM): 130 NaCl, 3.5 KCl, 1.2 NaH_2PO_4, 1 $MgCl_2$, 1.5 $CaCl_2$, 24 $NaHCO_3$ and 10 glucose, pH 7.2–7.4, at RT and bubbled with carbogen. When required, slices were transferred to a recording chamber superfused with aCSF, bubbled with carbogen (30°C and perfusion speed of 2 ml/min). Pharmacological manipulations were delivered by bath application of drugs through the perfusion system for 10 minutes. Stock solutions were generated, aliquoted, and stored at -20°C. On an experiment day, stock solution was added to the aCSF to achieve the desired final concentration (in μM): 10 bumetanide (NKCCI inhibitor), 10 VU0463271 (KCC2 inhibitor), 1 TTX (voltage-gated sodium channel blocker), 1 CPG55845 ($GABA_BR$ antagonist), 3 bicuculline ($GABA_AR$ antagonist). All drugs were purchased from Tocris Bioscience.

Gramicidin perforated patch clamp recordings

To preserve a neuron's $[Cl^-]_i$ and infer transmembrane gradients for chloride, gramicidin perforated patch clamp recordings were performed [56]. Patch pipettes were pulled from standard wall borosilicate glass capillaries (2-5 MΩ) and filled with a high KCl based internal solution to be able to monitor the integrity of the perforated patch, and containing (in mM): 135 KCl, 4 Na_2ATP, 0.3 Na_3GTP, 2 $MgCl_2$, and 10 HEPES. Osmolarity was adjusted to 290 mOsM and the pH was adjusted to 7.35 with KOH. Gramicidin (Calbiochem) was dissolved in dimethylsulfoxide (DMSO) to achieve a stock concentration of 4 mg/ml. This was then diluted into the internal solution on the day of the experiment to achieve a final concentration of 80 μg/ml. The resulting solution was vortexed for 40 s, sonicated for 10 s, then filtered through a 0.45 μm pore cellulose acetate membrane filter (Nalgene) and used immediately.

Neurons were visualized under a 60x water-immersion objective (Olympus BX51WI). Recordings were performed with an Axopatch 1D amplifier (Molecular Devices), acquired using WinWCP Strathclyde software (V.3.9.7; University of Strathclyde) and stored for off-line analysis. Recordings were made when the series resistance had stabilized to approximately 100 MΩ (approximately 30 min after gigaseal formation). $[Cl^-]_i$ measurements were performed by activating either $GABA_A$ or glycine receptors by delivering short 'puffs' of either GABA (Tocris Bioscience, 100 μM) or glycine (Tocris Bioscience, 100 μM) via a patch pipette placed in the vicinity of the cell soma and

connected to a picospritzer (5–10 psi for 20–40 ms; General Valve). Puffs were delivered at a low frequency (15 s intervals) to ensure recovery of chloride homeostasis. The polarity of GABAergic responses was monitored by activating $GABA_A$Rs in current clamp mode at resting membrane potential (I=0). $EGABA_A$ measurements were performed in voltage clamp mode from a holding potential of -70 mV. Test voltage ramps (a saw-tooth, down-up function of 500 ms duration, with a minimum of -90 mV and maximum of -50 mV) were delivered at baseline (control ramp) and near the peak of the GABA-evoked current (GABA ramp; Extended Data Fig. 1a). For each neuron, I-V curves of the control and GABA ramps were generated using linear fits after 70% series resistance correction. $EGABA_A$ was defined as the membrane potential at which the control and GABA ramp currents intersected, which was equivalent to the membrane potential at which the difference between the GABA and control ramp currents was equal to zero (Extended Data Fig. 1b). $EGABA_A$ for each data point was a mean of 10 measurements.

To perform *in vivo* perforated patch clamp recordings, we bred Gad2tm2(cre)Zjh/J mice (Gad2-IRES-Cre; Jackson Laboratory, Maine, USA) and B6;129S-Gt(ROSA)26Sortm32(CAG-COP4*H134R/EYFP)Hze/J mice (Ai32; Jackson Laboratory, Maine, USA), to produce heterozygous mice expressing ChR2(H134R)-YFP in all main subclasses of GABAergic interneurons. Head plate fixation was performed under stereotactic surgery on male mice aged 6 weeks. A custom-designed aluminium head-plate with a 7 mm well was bonded to the skull with adhesive glue (Loctite) and dental cement (Super-Bond). The well was then covered with silicone sealant (Kwik-Cast) and the animal was recovered. Recordings were performed at 8 weeks of age and, during the week prior to recording, each animal was habituated to head-fixation for increasing time intervals of up to 60 minutes. Animals were studied at ZT3 on the day of recording, having either just experienced the standard 3-hour SD protocol (‘ZT3-SD’) or having been allowed to sleep during the equivalent period (‘ZT3’). To prepare the brain for the perforated recordings, the animal was briefly anaesthetized (less than 20 min) with isoflurane and mounted onto a stereotaxic frame. The silicone sealant was removed, a craniotomy and durectomy were performed, and the site covered with 2% agarose. The animal was then recovered and mounted onto the head-fixation setup and perforated patch clamp recordings were performed using glass pipettes (5-8 MΩ) filled with the same high chloride gramicidin solution as described for *in vitro* recordings, with the addition of 15 mM Alexa Fluor 594 (Thermo Fisher). Pipettes were mounted into an ‘Optopatcher’ pipette holder (A-M Systems)[57], which permitted laser light transmission via an embedded 50 μm fibre (Thorlabs), connected to a 473 nm laser (MBL-FN-473-150mW, CNI Laser). To standardize network activity at the recording site, the AMPA receptor antagonist NBQX (100 μM, 250 nL, Torcis) was injected via a micropipette. A ground electrode (Multichannel Systems) was placed in the recording well and two-photon guided perforated shadow patch clamp recordings were performed. Briefly, patch pipettes with positive pressure (200-300 mBar) were lowered onto the brain surface under 4x magnification. The pipette was then visualized under 40x magnification, inserted into the brain (200-300 μm from the surface), and the positive pressure lowered to 20-30 mBar. The pipette was then located using a custom-built two-photon microscope, which consisted of a modified confocal scan unit (Olympus FV300) coupled to a Ti:Sapphire laser (Newport Spectra-Physics Mai Tai HP; wavelength 820

nm, power 50 mW). A neuron was approached and when consistent changes in electrode resistance appeared, the positive pressure was released and the holding potential clamped at -70 mV in voltage-clamp mode to assist gigaseal formation. Once the series resistance dropped below 100 MΩ, the recording configuration was switched to current clamp mode. Perforations were also confirmed visually by monitoring the lack of Alexa dye diffusion into the cell. To probe synaptic GABA responses, 10 ms light pulses were delivered every 10 s (30 times). Data were acquired using a Multiclamp 700B amplifier (Molecular Devices), processed by a 50 Hz noise eliminator (HumBug, Digitimer).

Western blotting

Animals were sacrificed at ZT3 having either experienced a 3-hour SD protocol or having been allowed to sleep during the equivalent period. Mouse somatosensory cortex was dissected and the tissue immediately flash-frozen in liquid nitrogen, then stored at -80°C until required. Tissue samples were homogenized in chilled Cell Lysis Buffer (Cell Signalling Technology) supplemented with HALT protease and phosphatase inhibitor cocktail (Thermo Scientific), vortexed, sonicated and incubated on ice for 30 min, followed by 10 min centrifugation at 4°C, 16,100 **g**. Total protein levels were quantified with a BCA protein assay (Thermo Scientific) and 40 μg per animal was loaded into a 6% SDS-PAGE gel for electrophoresis. Gels were immunoblotted onto Protran nitrocellulose membranes (Sigma Aldrich), incubated in Intercept (TBS) blocking buffer (LI-COR) for 1 h at RT, and finally incubated overnight at 4°C with primary antibodies against NKCC1 (T4, 1:1000, DSHB) and tubulin (anti-Tuj1, 1:5000, Biolegend, 801201) diluted in the blocking buffer with 0.1% tween. The following day, membranes were washed using TBS containing 0.1% tween and incubated with IRDye 680RD secondary antibody (1:5000, LI-COR), diluted in the blocking buffer containing 0.01% SDS and 0.1% tween at RT for 1 h, and shielded from light. Membranes were washed with TBS and imaged with a blot scanner (LI-COR). Each animal's NKCC1 signal was normalized to its corresponding tubulin signal.

Quantitative immunohistochemistry

To validate the NKCC1 antibody, in utero electroporation was performed on mouse embryos at embryonic day 13 (E13) to induce shRNA knockdown of NKCC1 in L5 pyramidal neurons within S1 [58]. Pregnant females were anaesthetised using isofluorane and analgesia (buprenorphine and meloxicam) was provided as required. The uterine horns were exposed by midline laparotomy and a plasmid DNA mixture was injected intraventricularly into the embryos using glass micropipettes, through the uterine wall and amniotic sac. The DNA comprised three plasmids: CAG-Cre to drive high expression of Cre recombinase, floxed tdTomato for conditional expression of tdTomato, and pSico for conditional expression of either shRNA-NKCC1 (sequence, ACACACTTGTCCTGGGATT) or shRNA-control (sequence, GCGCGATAGCGCTAATAATTT). pCAG-Cre was a gift from Connie Cepko (Addgene plasmid # 13775; http://n2t.net/addgene:13775; RRID:Addgene_13775), pAAV-FLEX-tdTomato was a gift from Edward Boyden (Addgene plasmid # 28306; http://n2t.net/addgene:28306; RRID:Addgene_28306), and pSico (pSico-shNKCC1) was a gift from Angelique Bordey (Addgene plasmid # 83027; http://n2t.net/addgene:83027; RRID:Addgene_83027), in which the shRNA-NKCC1 sequence was replaced with the shRNA-control sequence. Total injected volume per embryo was ~1 μl, plasmids were at

a 1:1:1 ratio, and final concentration of each plasmid was ~1 μg/μl. The anode of a 5 mm Platinum Tweezertrode (BTX) was placed over the dorsal telencephalon outside the uterine muscle. Five pulses (50 ms duration separated by 950 ms) at 36 V were delivered with an ECM 830 pulse generator (BTX). The uterine horns were placed back inside the abdomen, the cavity filled with warm physiological saline, and the abdominal muscle and skin incisions were closed. Postnatal offspring were sacrificed and the brains stored in 4% paraformaldehyde (PFA, Sigma Aldrich) for 48 h before sectioning coronally at 50 μm on a vibrating microtome (Microm). For quantitative immunohistochemistry in ZT3 and ZT3-SD animals, mice were anaesthetized and underwent cardiac perfusion with PBS and 4% PFA at ZT3, having either experienced the standard 3-hour SD protocol ('ZT3-SD') or having been allowed to sleep during the equivalent period ('ZT3'). Brains were stored in 4% PFA for an additional 48 h and sectioned coronally at 50 μm.

To perform immunohistochemistry, sections were washed three times in PBS for 5 min, then blocked in 20 % normal goat serum (NGS, Sigma Aldrich) in 0.1% Triton-X (Thermo Fisher) in PBS (PBST) for 2 h at RT. Sections were washed in PBS and incubated with primary antibody diluted in 0.1% PBST at 4 °C for 48 **h**. Primary antibodies included an phospho-NKCC1 antibody raised against a linear diphosphopeptide corresponding to Thr212 and Thr217 of NKCC1 (1:250, rabbit, Merck Sigma-Aldrich, ABS1004, Lot: 3224588) and an anti-NeuN antibody (1:500, mouse, Merck Sigma-Aldrich, MAB377, Lot: 2326372). Slices were washed in PBS and were incubated for 2 h with secondary antibodies diluted in 0.1% PBST at RT. Secondary antibodies included an anti-rabbit Alexa fluor 488 (1:1000, goat, Thermo Fisher, A11034, Lot: 1531670), anti-mouse Alexa fluor 647 (1:1000, goat, Thermo Fisher, A21240, Lot:2349091), and anti-rabbit Alexa fluor 647 antibody (1:500, goat Thermo Fisher, A21244, Lot:2390713). Sections were mounted on slides with VectaShield (Vectorlabs). Fluorescent images were acquired with a LSM 880 confocal microscope (Zeiss) equipped with 488 nm, 561 nm, and 633 nm lasers and a 20x water-immersion objective (W Plan-Apochromat) using ZEN software (Zeiss). To measure fluorescence signals from layer 5 neurons, sections were analysed blind to condition. Confocal images at a single optical plane were collected at a depth of 10 μm from the surface of the section. Automated fluorescence analysis was performed using FIJI (ImageJ). Regions of interest were drawn around neuronal soma, the mean signal intensity calculated, and a background signal subtracted based on measurements from adjacent areas that did not contain soma.

Recordings in freely moving mice

For chronic electroencephalogram (EEG) and electromyogram (EMG) recordings, custom-made headstages were constructed by connecting three stainless steel screw electrodes (Fine Science Tools) and two stainless steel wires, to an 8-pin surface mount connector (8415-SM, Pinnacle Technology Inc., Kansas). For chronic *in vivo* LFP recordings combined with drug infusion, custom-designed cannulae (26 gauge) were coupled to two-channel insulated electrode wires (0.125 mm; C315G, PlasticsOne), and connected to the same 8-pin surface mount connector. For 4-channel LFP and multi-unit activity recordings combined with optogenetics, a tetrode in diamond configuration (25 μm spacing) was coupled with a fibre optic (200 μm, 0.22 NA, fibre terminates 100 μm above top site;

Q1X1-tet-3mm-121-OCQ4LP, NeuroNexus) and connected to a zif-clip compatible adapter (CQ4-Z32, NeuroNexus).

Device implantation and viral injections were performed at 7-8 weeks of age using stereotactic surgery, aseptic technique, isoflurane anaesthesia (3-5% for induction and 1-2% for maintenance) and constant body temperature monitoring. Analgesia was provided at the beginning of surgery and during recovery (buprenorphine and meloxicam). A craniotomy was performed over the right frontal cortex (AP +2 mm, ML +2 mm from Bregma), right occipital cortex (AP -3.5 mm, ML +2.5 mm from Bregma), left somatosensory cortex (AP -1.2 mm, ML -3 mm from Bregma) and the cerebellum (~-1.5 mm posterior from Lambda, ML 0). For EEG recordings, a screw was fixed over both the right frontal and occipital cortex. For LFP and multi-unit activity recordings, either a cannula coupled with electrodes or a tetrode coupled with fibre optic, was implanted into L5 of left somatosensory cortex (700 nm depth). EEG, LFP and multi-unit activity signals were referenced to the cerebellum screw. For EMG recordings, wire electrodes were inserted into the left and right neck muscles and one signal acted as reference to the other. All implants were secured using a non-transparent dental cement (Super-Bond). To express opsins, an AAV1-CamKiia-eNpHR3.0-EYFP or AAV1-CamKii-ArchT-GFP virus was injected, before device implantation, into left somatosensory cortex (40 nl/min, 350 nl at 700 nm depth and 350 nl at 400 nm depth) using a Hamilton syringe (5 μl, 32-gauge) and an infuse/withdrawal pump (Harvard Apparatus). Animals were randomly assigned to receive the different viruses. pAAV-CamKiia-eNpHR3.0-EYFP was a gift from Karl Deisseroth (Addgene viral prep #26971-AAV1; http://n2t.net/addgene:26971; RRID:Addgene_26971) while pAAV-CamKiia-ArchT-GFP was a gift from Edward Boyden (Addgene viral prep #99039-AAV1; http://n2t.net/addgene:99039 ; RRID:Addgene_99039). Animals were allowed to recover for at least 1 week before recordings, or 4-8 weeks to allow for opsin expression.

Halorhodopsin and Archaerhodopsin were activated with a 561 nm, 50 mW solid-state laser (Cobolt) connected to a 200 μm core patch cord LC-Ferrule (NeuroNexus), which was fixed to the implanted 200 μm fibre optic via a ceramic sleeve. Maximum light power at the fibre optic tip was 30-40 mW and light intensity was further reduced using neutral density filters (ND filters 0.2-0.3; Thorlabs). When mice entered NREM sleep between ZT3 to ZT9, the experimenter activated a protocol consisting of 5 cycles of 20-60s light ON, followed by 40s light OFF.

Continuous *in vivo* data acquisition

Animals were moved to a recording chamber and housed individually in a Plexiglas cage (20.3 x 32 x 35 cm). Recordings were performed using a 128-channel Neurophysiology Recording System (Tucker-Davis), acquired using the electrophysiological recording software, Synapse (Tucker-Davis), and stored locally for offline analysis. EEG, EMG, and LFP signals were continuously recorded with a sampling rate of 305 Hz. Extracellular multi-unit activity was recorded at a sampling rate of 25 kHz and filtered between 300 Hz – 5 kHz. Spike thresholds were set manually during the sleep period and used to identify waveform epochs containing spikes (0.48 ms before and 1.34 ms after threshold crossing).

Vigilance state scoring

LFP, EEG, and EMG data was resampled at 256 Hz and converted into the European Data Format (EDF). The data was pre-processed for automated scoring by computing the spectrograms of the EEG and EMG traces using the multitaper approach [59], as implemented in the lspopt module (1 s segments with no overlap, other parameters at default values). Signals in the 0-1 Hz frequency range were removed as these exhibited drift due to animal locomotion. Signals between 45-55 Hz and above 90 Hz were also removed, as these were affected by 50 Hz electrical noise. A log x + 1 transformation was then applied to map the heavy-tailed distribution of power values onto a more normal distribution. Finally, the values in each frequency bin were normalized to a Z-score to ensure that the downstream classification assigned equal weight to all signals across frequencies. To determine vigilance state, we used a hidden Markov model (HMM) to compute the posterior probability of each state based on (i) the probability of each state given the sample, and (ii) the probability of each state given the likelihood of states in previous time points. Both sets of probability distributions were estimated based on training data that had been annotated by human scorers. Linear discriminant analysis (LDA) implemented in scikit-learn [60] was used to reduce the dimensionality of the pre-processed and combined spectrograms of the EEG and EMG traces, down to a two-dimensional signal. An HMM with multivariate normal sample distributions for each state and a sparse transition matrix was constructed, and the Viterbi path was computed using the pomegranate module [61] to determine the maximum likelihood state sequence. To establish performance levels for the automated method, approximately half of the data sets (55 of the 92 x 24 h recordings from 16 animals) were partitioned into 4 s epochs and manually scored using SleepSign for Animals software (SleepSign, Kissei Comtec) with criteria as described previously [62]. Automated and manual vigilance state scoring showed a very high correspondence, with 97% match for NREM sleep epochs, 91% match for REM sleep epochs, and 98% match for wake epochs. Spectral power was generated from the automated vigilance state scoring, which ensured that the experimenter was blinded from the analysis.

In vivo drug infusion

Stock solutions were made by dissolving drugs in DMSO to reach a concentration of 10 mM, aliquoted and stored at -20°C. Tubing and internal cannulae were flushed with 70% ethanol and sterile saline the day before the experiment. On the day of the experiment, drugs were prepared by dissolving stock solutions in sterile saline to reach a final concentration of (in μM): 55 Bumetanide and 55 VU VU0463271. The vehicle contained the same concentration of DMSO in sterile saline. Each infusion solution was loaded into a heavy wall polyethylene tubing (PE50 - C313CT; PlasticsOne) that allowed the animal to move freely, and was connected to an internal cannula (C315I; PlasticsOne) and captive collar (PlasticsOne). A small air bubble was loaded into the tubing, just before connecting to a 1 μl Hamilton syringe (26 gauge needle). In awake mice, the internal cannula was inserted into the implanted cannula at either the beginning of light onset or at the beginning of a SD protocol, by unscrewing the dummy cannula, gently restraining the animal and covering the eyes to evoke brief freezing behavior. The captive collar was then tightened to secure the internal cannula to the implanted cannula. Infusion was performed using an infuse/withdrawal pump (Harvard apparatus; 700 nl at a speed of 40 nl/min) and monitored

Europe PMC Funders Author Manuscripts

by tracking the progression of the air bubble through the tubing. Under these injection conditions, no evidence for epileptiform activity was observed in EEG or LFP recordings [63]. Once the infusion experiment was completed, the internal cannula was disconnected and the dummy cannula replaced. The order of vehicle and drug infusions was counterbalanced and randomized.

Data analysis and statistics

EEG and LFP spectral power were generated using the Spectrogram function in Matlab, with 0.25 Hz resolution. Signals between 0.5-20 Hz were analysed as changes in this range have been most consistently related to sleep pressure, and this avoided potential contamination by 50 Hz electrical noise. Spectral power for each frequency bin was normalized to the average power over a 12 h baseline period recorded the day before the experiment, during which the animal was undisturbed. To investigate neuronal recruitment to different phases of a slow wave, the LFP signal during NREM sleep was classified into ON periods (when neurons are more likely to spike) and OFF periods (when most neurons are silent). Detected spikes were plotted on the corresponding Hilbert-transform of the LFP signal (bandpass filtered: 0.5-12 Hz). As recordings were made extracellularly and from deep cortical layers, the OFF period was defined as the upward phase (30 -150° angle) of high amplitude slow-waves (>30% LFP mean amplitude), and the remaining phase was classified as the ON period (Extended Data Fig. 8g,h). These criteria detected a mean of 15.7 ± 2.3 spikes per s during ON periods and 1.87 ± 0.4 spikes per s during OFF periods. All statistical tests were performed using InStat (Graphad). No statistical methods were used to pre-determine sample sizes, but our sample sizes are similar to those reported in previous publications[10,18,29,32,43]. Data was assessed for normality using a Kolmogorov-Smirnov test, and then the appropriate parametric or non-parametric test was performed. Appropriate correction such as the Welch's correction were applied when comparing data with unequal standard deviations. All tests were two-tailed, with a confidence level of at least a 95%. Effect size was estimated using Cohen's D test, computed using the 'computeCohen_d' function in Matlab and was denoted as 'd'. Unless stated otherwise, values in the text represent mean ± stdev. No animals or data points were excluded from the analyses.

Neuronal network simulation

A simple network model was used to explore the effect of $EGABA_A$ upon neuronal recruitment during ON and OFF periods. The network was constructed using the neuron simulator Brian 2 [64] and comprised 400 glutamatergic neurons and 100 GABAergic neurons. Each neuron was modelled as a single compartment, current-based leaky integrate-and-fire neuron. Free parameters were set as follows: -60 mV resting potential, 200 pF membrane capacitance, 20 ms membrane time constant, 5 ms excitatory post-synaptic potential decay time constant, 10 ms inhibitory post-synaptic potential time constant, and -50 mV spike threshold. The glutamatergic neurons received synaptic connections from the glutamatergic and GABAergic neurons; the GABAergic neurons received connections from the glutamatergic neurons. Within these constraints, the connection probability was set uniformly to 5%, excitatory synaptic weights were set to 0.3 nS and inhibitory weights were initialized at 0.1 nS. To simulate ON-OFF periods, all neurons in the network received a time-varying excitatory external input consisting of a square wave of a particular frequency.

Europe PMC Funders Author Manuscripts

The external input comprised two components: the first was common to all neurons and switched between 0 and 100 pA at the defined frequency; the second was a background noise current that was unique to each neuron and varied on a 10 ms timescale, with values drawn from a normal distribution (mean and standard deviation of 50 pA). Before running a simulation, homeostatic inhibitory synaptic plasticity was used to establish a balance of excitatory and inhibitory inputs to each neuron [65], and then synaptic weights were frozen. Only $EGABA_A$ was then varied and each simulation was repeated 10 times.

Novel object recognition

A recognition memory paradigm was used to test novelty preference within either the somatosensory modality ('tactile task') or olfactory modality ('odor task'). The paradigm was performed in a white rectangular arena (40 cm x 60 cm x 40 cm), under low levels of red light to prevent visual cues. The arena was wiped down with 70% ethanol between sessions. Before the day of the experiment, mice underwent a habituation protocol that involved being placed in the arena for 10 min, on 3 consecutive days. Tactile objects were 3D-printed and varied in shape and surface texture, but were comprised of the same material to avoid odor cues. Exploration time for the tactile objects was defined as the period that the animal's head was oriented towards the object and the whiskers or paws were in contact with the object. Odor objects such as tea leaves, cinnamon powder or orange peel, were each placed at the bottom of small, open glass jars. This ensured that the odor objects were out of the animal's reach, to avoid gustatory and tactile cues. Exploration time for the odor objects was defined as the period the animal spent sniffing the top of the jar.

On the day of the experiment, each sample period (i.e. T1) involved placing the animal at one edge of the arena, opposite two identical objects that were each positioned 10 cm away from adjacent corners (Fig. 8b). The animal's behavior was then monitored until exploration time reached a total of 60 s or 30 s for the tactile or odor task, respectively. The animal was then returned to its home cage for a 3 min interval, during which the arena was cleaned and a different copy of the familiar object (from T1) was placed in one of the corners, and a novel object was placed in the other corner. The test period (i.e. T2) involved placing the animal at the same starting point in the arena and monitoring behavior over a period of 5 min. Novelty preference was calculated as the ratio between the time spent exploring the novel object and the total exploration time (Novel/(Novel+Familiar)). Every animal was subjected to both control and treatment conditions on different experimental days. The order of vehicle versus drug infusion, and the identity and position of familiar versus novel objects, was each counterbalanced and the experimenter was blinded to the treatment condition.

Europe PMC Funders Author Manuscripts

Extended Data

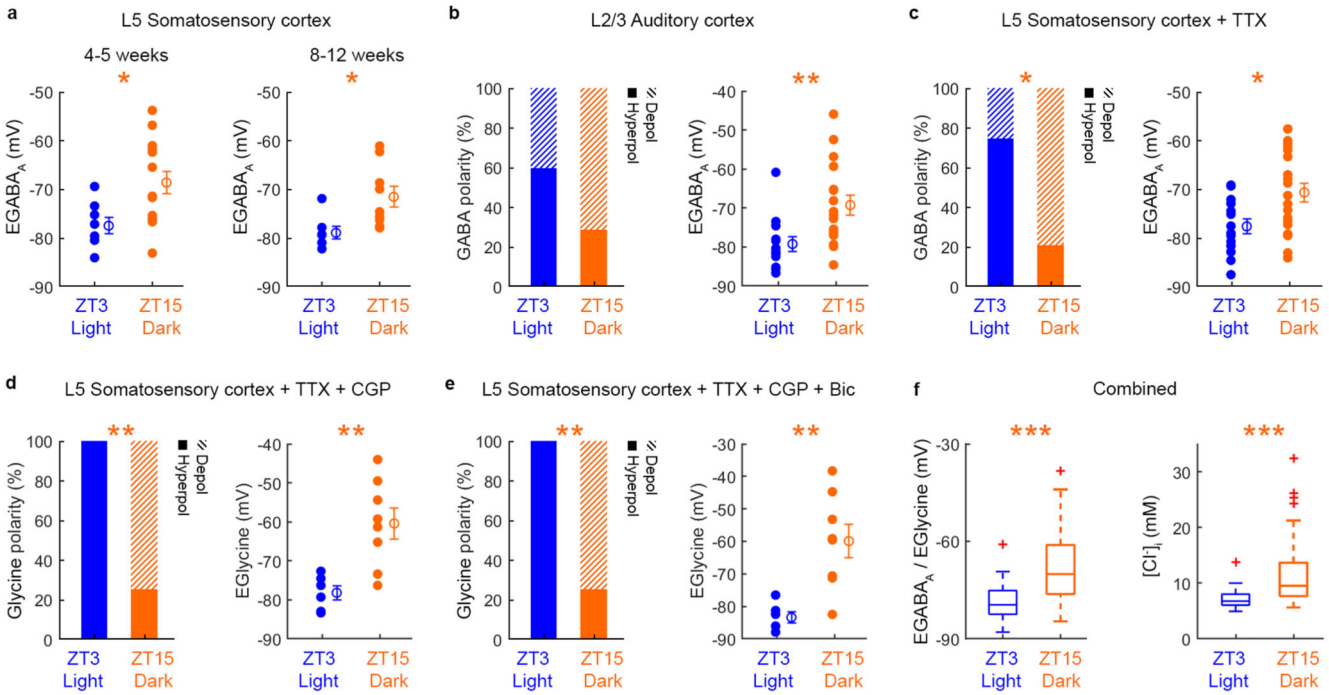

Extended Data Fig. 1.

Cortical pyramidal neurons exhibit diurnal variations in EGABA$_A$. Activating Cl$^-$-permeable receptors in current clamp, and estimating the equilibrium potential of GABA$_A$Rs (EGABA$_A$) or glycine receptors (EGlycine) under different recording conditions, supports the conclusion that cortical pyramidal neurons exhibit diurnal variations in intracellular chloride regulation. **a**. EGABA$_A$ shows diurnal variation in both juvenile and adult somatosensory cortex. EGABA$_A$ was more depolarized at ZT15 than at ZT3 in L5 pyramidal neurons from mice aged 4-5 weeks (left; *p=0.015, unpaired t-test; t=2.66; df=21; d=1.16; blue: 8 neurons, 8 slices, 2 animals; orange: 15 neurons, 15 slices, 3 animals) and in mice aged 8-12 weeks (right; *p=0.016, unpaired t-test; t=2.74; df=14; d=1.38; blue: 7 neurons, 7 slices, 5 animals; orange: 9 neurons, 9 slices, 5 animals; Multi group comparison: p=0.0008 for ZT time effect, p=0.27 for age effect, p=0.75 for interaction between ZT time and age effect; 2-way Anova). **b**. The proportion of L2/3 pyramidal neurons in brain slices from auditory cortex that exhibited a depolarizing GABA$_A$R response at ZT3 and ZT15 (left; p=0.3, Fisher's exact test; blue: 10 neurons, 10 slices, 7 animals; orange: 7 neurons, 7 slices, 4 animals). EGABA$_A$ in L2/3 pyramidal neurons of auditory cortex was more depolarized at ZT15 than at ZT3 (right; **p=0.006, unpaired t-test; t=2.97; df=28; d=1.09; blue: 13 neurons, 13 slices, 7 animals; orange: 17 neurons, 17 slices, 7 animals). EGABA$_A$ data from Fig. 1. **c**. The same pattern was observed when action potential activity was blocked by applying TTX throughout the recordings. A higher proportion of L5 pyramidal neurons exhibited a depolarizing GABA$_A$R response at ZT15, compared to ZT3 (left; *p=0.026, Fisher's exact test; blue: 8 neurons, 8 slices, 4 animals; orange: 14 neurons, 14 slices, 5 animals). EGABA$_A$ was more depolarized at ZT15 than at ZT3 when

action potential activity was blocked throughout the recordings (*p=0.0109, unpaired t-test; t=2.708; df=31; d=0.95; blue: 14 neurons, 14 slices, 7 animals; orange: 19 neurons, 19 slices, 7 animals). $EGABA_A$ data from Fig. 1. **d**. Activating Cl^--permeable glycine receptors, in the presence of TTX and the GABAB receptor blocker CGP55845 (CGP), revealed the same pattern. A higher proportion of L5 pyramidal neurons exhibited a depolarizing glycine response at ZT15 than at ZT3 (left; **p=0.0097, Fisher's exact test; blue: 6 neurons, 6 slices, 3 animals). EGlycine was more depolarized at ZT15 than at ZT3 (right; **p=0.0033, unpaired t-test; t=3.663; df=12; d=1.98; blue: 6 neurons, 6 slices, 3 animals; orange: 8 neurons, 8 slices, 4 animals). **e**. The same pattern was observed when GABAA receptors, GABAB receptors and action potential activity were all blocked. A higher proportion of L5 pyramidal neurons exhibited a depolarizing glycine response at ZT15 than at ZT3 (left; **p=0.0097, Fisher's exact test; blue: 6 neurons, 6 slices, 3 animals; orange: 8 neurons, 8 slices, 4 animals). EGlycine was more depolarized at ZT15 than at ZT3 (right; **p=0.0026, unpaired t-test; t=4.313; df=8; d=2.04; blue: 6 neurons, 3 animals; orange: 8 neurons, 4 animals). Data represent mean ± sem. f. Across all recordings conditions (a total of n=57 neurons from 57 slices, 28 animals at ZT3 and 75 neurons from 75 slices, 30 animals at ZT15), the estimated difference in $EGABA_A$/EGlycine between ZT3 and ZT15 was 11.1 mV (left; ***p<0.0001, unpaired t-test with Welch correction; t=7.98; df=115; d=1.29). Using the Nernst equation and treating $EGABA_A$/EGlycine as an estimate of the equilibrium potential for Cl^-, this would indicate a shift in $[Cl^-]_i$ of approximately 4.4 mM, (right; ***p<0.0001, Mann-Whitney Test; d=1.08). Center line: median, box limits: 25th and 75th percentile, whiskers: non-outlier min and max, outlier: 1.5 x interquartile range away from the bottom or top of the box. Data represent mean ± sem. All tests are two sided.

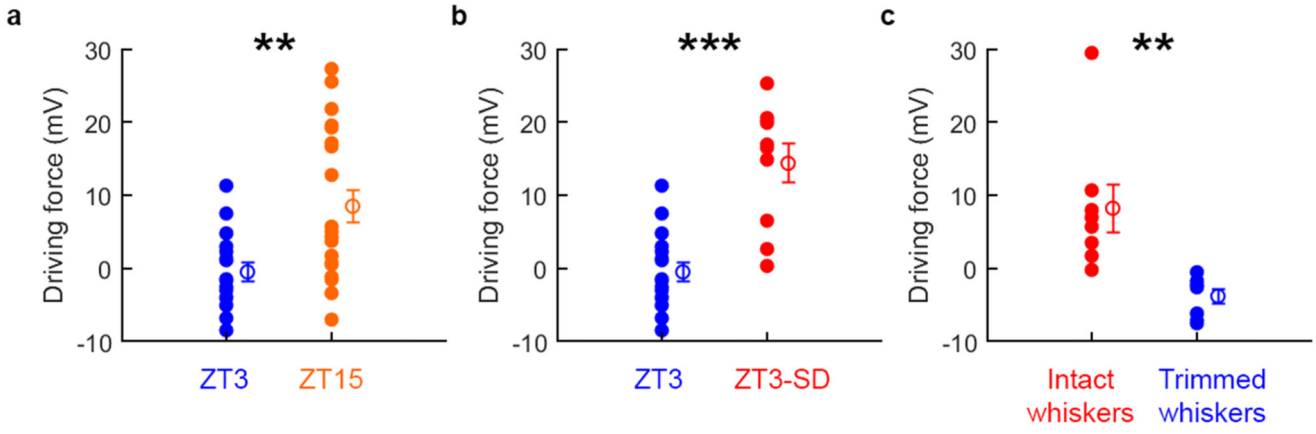

Extended Data Fig. 2. Diurnal and sleep-wake dependent variations in $EGABA_A$ alter the $GABA_AR$ driving force.

a. The $GABA_AR$ driving force was calculated as the difference between $EGABA_A$ and the neuron's resting membrane potential. The $GABA_AR$ driving force was significantly more depolarizing at ZT15 than at ZT3 in L5 pyramidal neurons (left; **p=0.003, Mann-Whitney test; d=1.08; blue: 17 neurons, 17 slices, 8 animals; orange: 21 neurons, 21 slices, 8 animals). **b**. The $GABA_AR$ driving force was more depolarizing at ZT3-SD when sleep pressure was high, than at ZT3 when sleep pressure was low (***p<0.0001, unpaired t-test;

t=5.57; df=25; d=2.22; red: 10 neurons, 10 slices, 4 animals; blue: same data as 'a'). **c**. Mice had their whiskers trimmed unilaterally at ZT3, when $EGABA_A$ is normally hyperpolarized, and were then subjected to 3 hours of SD (as in Figure 2i). The $GABA_AR$ driving force was more depolarizing in the hemisphere contralateral to the intact whisker input, compared to the hemisphere contralateral to the trimmed whisker input (**p=0.0078, Wilcoxon matched-pairs signed-ranks test; d=1.38; 8 neuronal pairs, 8 slices, 3 animals). Data represent mean ± sem. All tests are two sided.

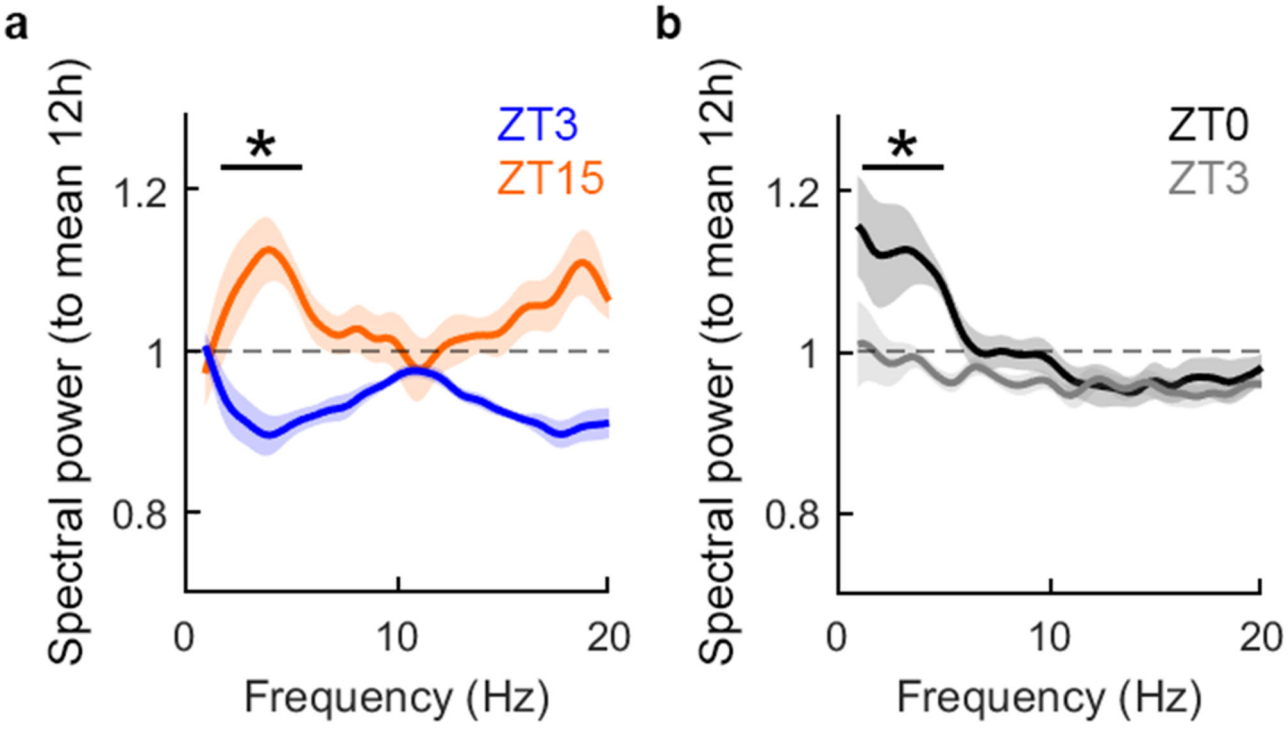

Extended Data Fig. 3. Levels of NREM SWA reflect recent sleep-wake history and indicate sleep pressure.

a. At ZT15, when mice have mainly been awake during the preceding 3 hours, spectral power shows higher levels of NREM SWA. At ZT3, when mice have mainly been asleep during the preceding 3 hours, lower levels of NREM SWA are observed (*p=0.0137, Wilcoxon matched-pairs signed-ranks test; d=1.49; blue: 10 days, 6 animals; orange: 10 days, 6 animals). SWA was monitored by frontal EEG and spectral power recorded over a two-hour period was normalized to the mean 12 hours light period. **b**. In a similar manner, mice at ZT0 that have mainly been awake during the preceding 3 hours show higher levels of NREM SWA compared to mice at ZT3, which have mainly been asleep during the preceding 3 hours (*p=0.0241, unpaired t-test with Welch's correction; t=2.996; df=6; d=1.73; black: 6 days, 6 animals; grey: 6 days, 6 animals). SWA was monitored by LFP via a tungsten wire targeted to L5 of primary somatosensory cortex (S1) and spectral power recorded over a two-hour period was normalized to the mean 12 hours light period. Data represent mean ± sem. All tests are two sided.

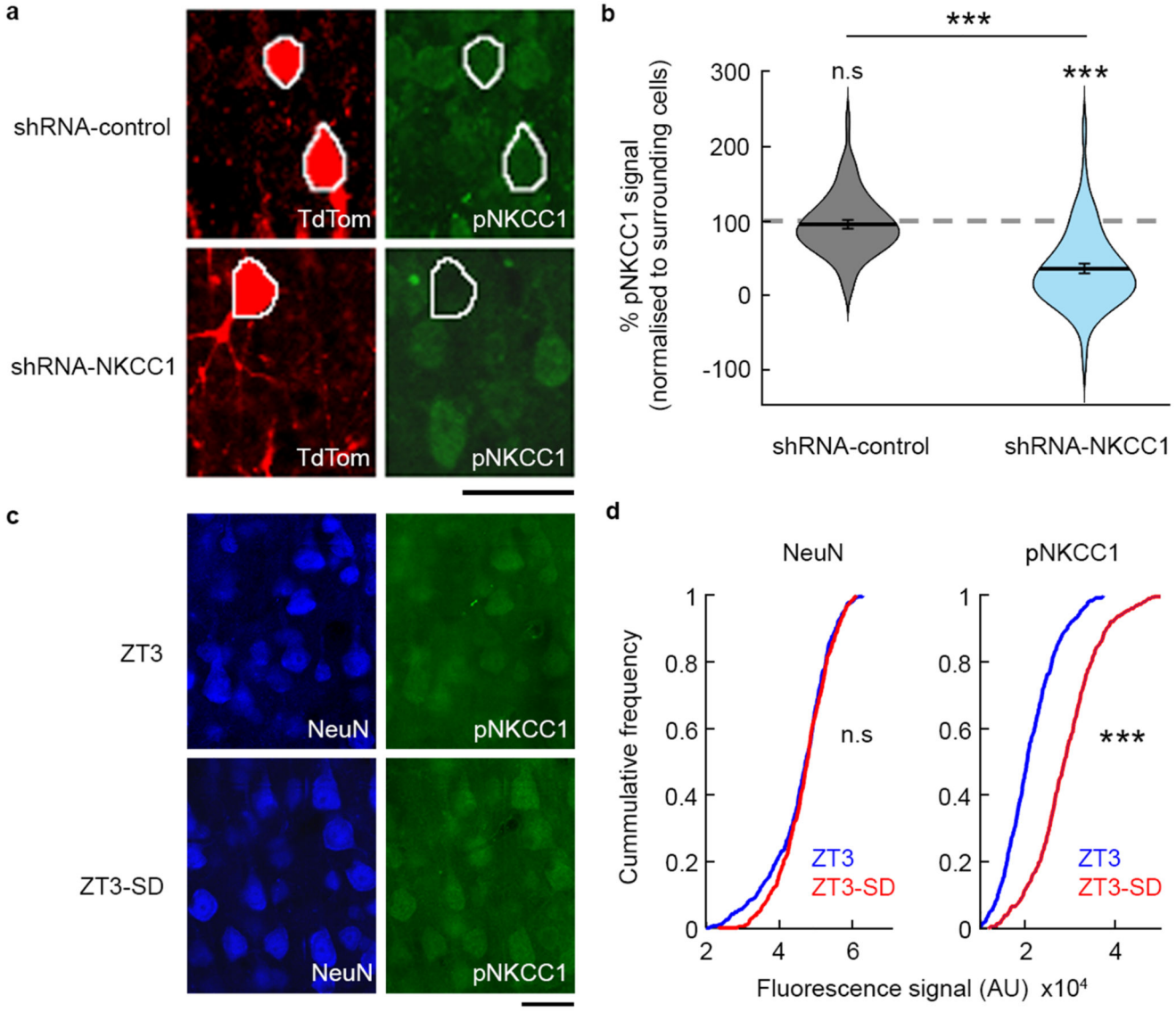

Extended Data Fig. 4. Sleep-wake history affects phospho-NKCC1 levels in layer 5 pyramidal neurons.

a. Confocal microscope images of immunofluorescence detected using a rabbit polyclonal antibody raised against a linear diphosphopeptide corresponding to Thr212 and Thr217 of NKCC1 (‘pNKCC1’; right) in L5 neurons that underwent in vivo shRNA knockdown of NKCC1 (‘shRNA-NKCC1’; bottom) or received control shRNA (‘shRNA-control’; top). Co-expression of TdTomato (‘TdTom’; left) was used to identify neurons transfected m **b**. Compared to surrounding non-transfectedμwith shRNA. Scale bar: 10 cells, the pNKCC1 signal was significantly reduced in shRNA-NKCC1 L5 neurons (light blue: $p<0.0001$, Wilcoxon signed rank test; $d=1.27$; 60 neurons, 4 slices, 4 animals), but not in shRNA-control neurons (grey: $p=0.21$, one sample t-test; $t=1.27$; $df=59$; $d=0.16$; 60 neurons, 3 slices, 3 animals), and the two groups were significantly different ($p<0.0001$, Mann-Whitney test; $d=1.27$). This supports the conclusion that the pNKCC1 antibody signal reflects

Europe PMC Funders Author Manuscripts

NKCC1 levels. Central line: mean; error bar: sem. **c**. Immunofluorescence signals for a neuron-specific marker ('NeuN; left) and NKCC1 (right) in layer 5 somatosensory cortex from mice 3 hours after light onset under control conditions (top; 'ZT3') or after a 3-hour sleep deprivation protocol (bottom; 'ZT3-SD'). Scale bar: m. **d**. Cumulative frequency plots of fluorescence (in arbitraryμ10 units) show higher pNKCC1 signal in the ZT3-SD condition compared to ZT3 (right; ***p<0.0001, Kolmogorov-Smirnov test; blue: 480 neurons, 6 slices, 3 animals; red: 480 neurons, 6 slices, 3 animals). This was not the case for the NeuN signal in the same population of neurons (left; p=0.11, Kolmogorov-Smirnov test). All tests are two sided.

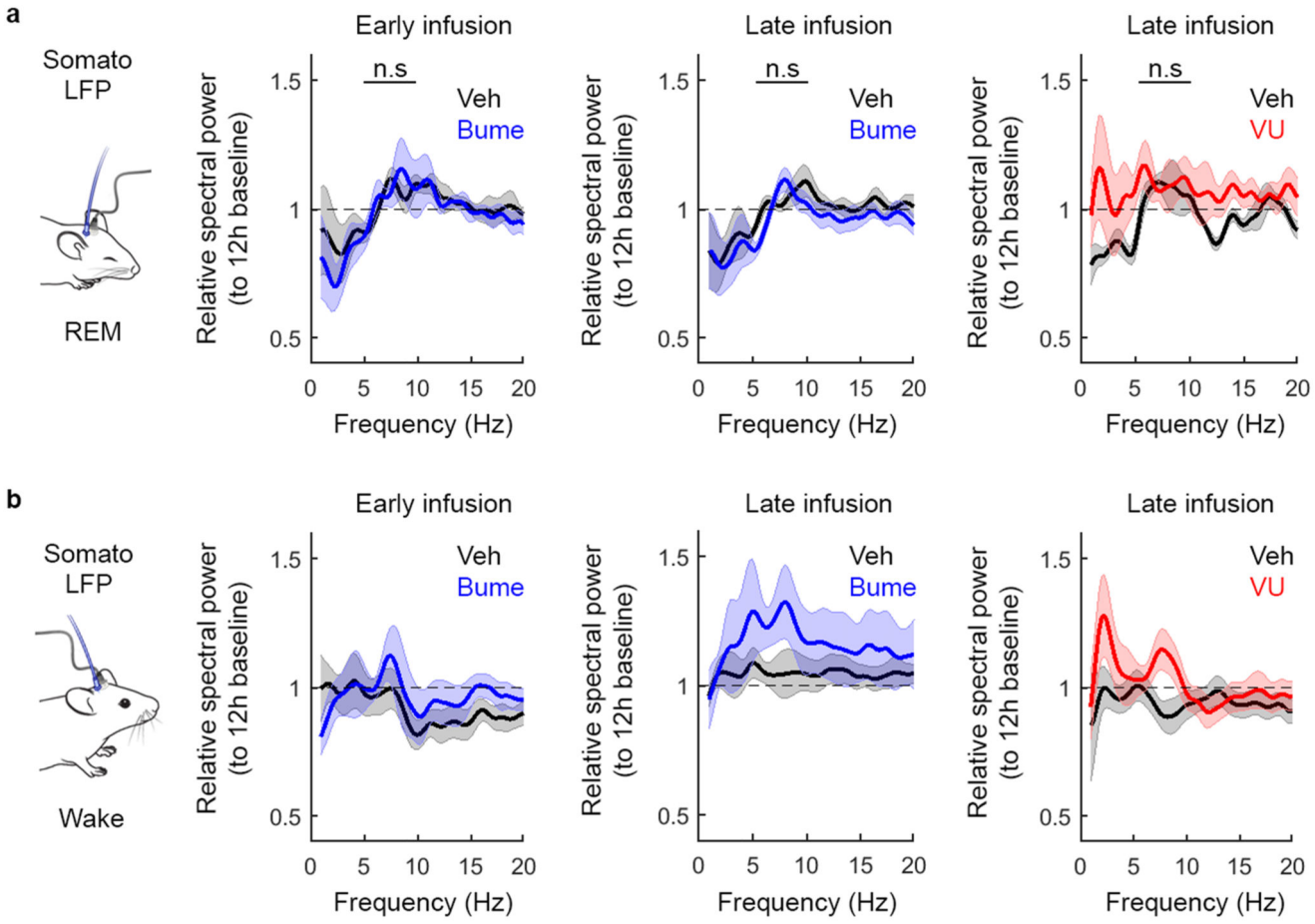

Extended Data Fig. 5. Spectral power during different vigilance states following bumetanide or VU infusion.

a-b. $[Cl^-]_i$ was manipulated at different time points by locally infusing blockers of NKCC1 (bumetanide) or KCC2 (VU) into S1. Spectral power from REM ('a') and wake ('b') LFP following infusion of vehicle or bumetanide during the early light period (left), vehicle or bumetanide during the late light period (middle), and vehicle or VU during the late light period (right). No differences were observed in theta frequency (5-10 Hz) during REM sleep following early bumetanide infusion (left; p=0.615, paired t-test; t=0.54; df=5; d=0.22; black and blue: 6 trials, 5 animals), late bumetanide infusion (middle; p=0.234,

Europe PMC Funders Author Manuscripts

paired t-test; t=11.35; df=5; d=0.55; black and blue: 6 trials, 5 animals), or late VU infusion (right; p=0.356, paired t-test; t=1.02; df=5; d=0.41; black and red: 6 trials, 4 animals). Data represent mean ± sem. All tests are two sided.

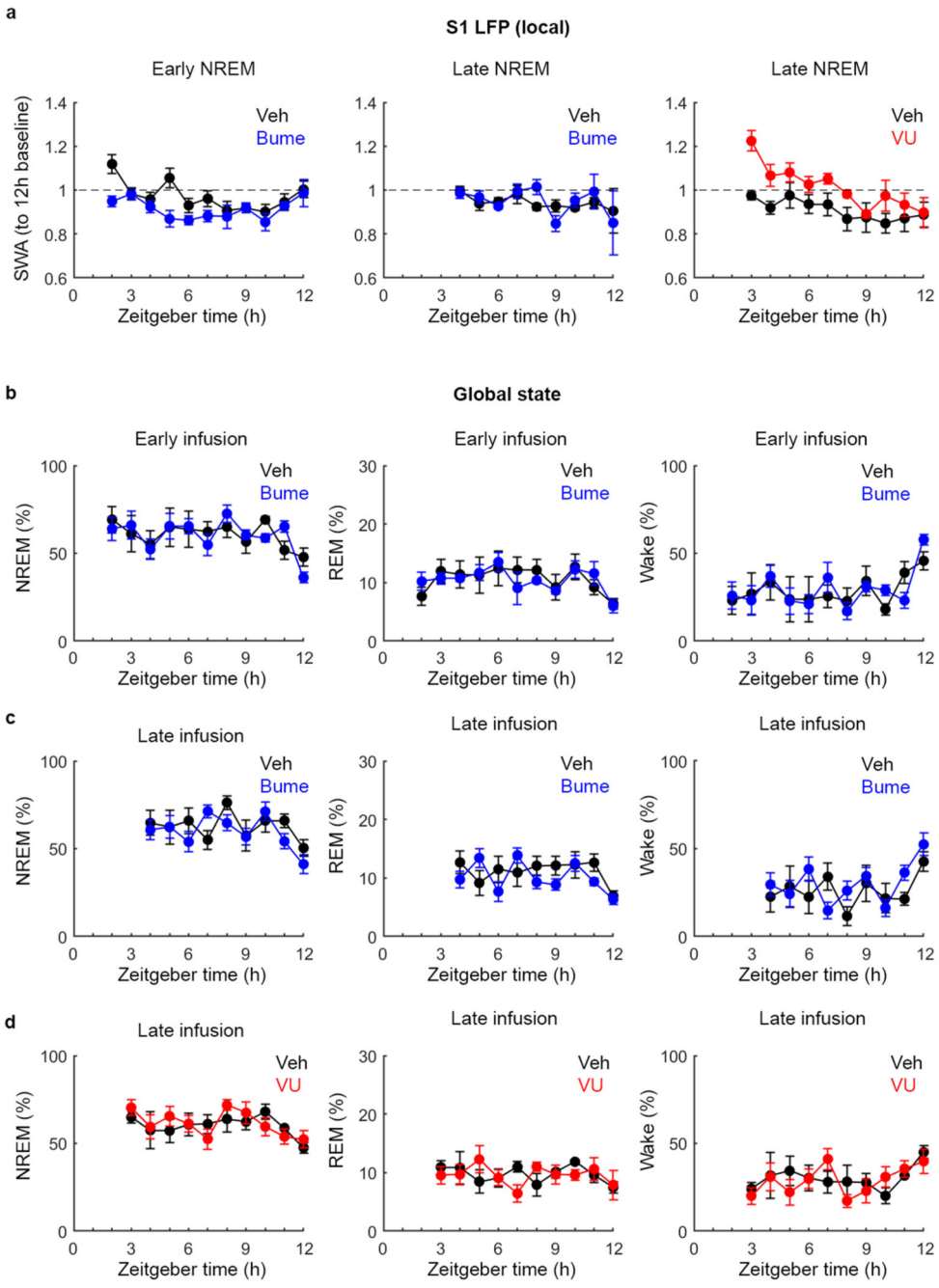

Extended Data Fig. 6.

Local NREM SWA and vigilance state distribution following bumetanide or VU infusion. $[Cl^-]_i$ was manipulated at different time points by locally infusing blockers of NKCC1 (bumetanide) or KCC2 (VU) into S1. **a**. Population data showing NREM SWA derived

from the S1 LFP (i.e. local) following infusion in mice that received vehicle or bumetanide during the early light period (left; black and blue: 6 trials, 5 animals), vehicle or bumetanide during the late light period (middle; black and blue: 6 trials, 5 animals), and vehicle or VU during the late light period (right; black and red: 6 trials, 4 animals). **b-d**. Population data on vigilance states (i.e. global state) showing the proportion of time spent in NREM sleep ('b'), REM sleep ('c'), and wake ('d') following local infusion of vehicle or bumetanide during the early light period (b, black and blue: 5 trials, 5 animals), vehicle or bumetanide during the late light period (c, black and blue: 5 trials, 5 animals), and vehicle or VU during the late light period (d, black and red: 5 trials, 4 animals). Data are plotted in 1-hour intervals. Data represent mean ± sem.

Europe PMC Funders Author Manuscripts

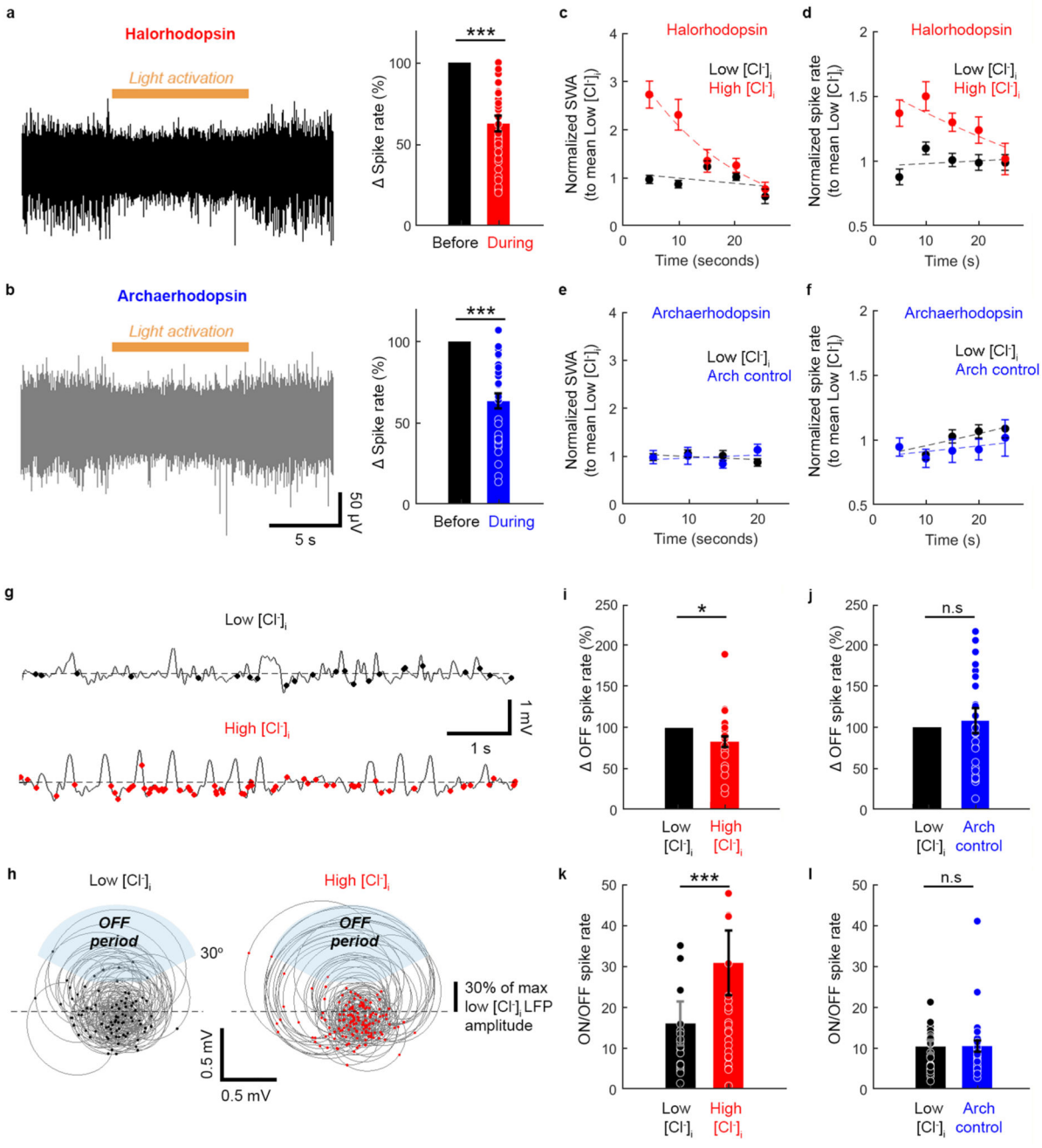

Extended Data Fig. 7. The effects of optical Cl^- loading on NREM SWA and neuronal recruitment during ON and OFF periods.

a. Multi-unit activity from an animal expressing halorhodopsin in pyramidal neurons of S1, during which a 10 s period of light was delivered during NREM sleep (left). Opsin activation was confirmed by decreased spike rate during light activation (right; ***p<0.0001, one sample t-test; t=7.88; df=36; d=1.26; 40 trials, 12 days, 5 animals). **b**. Multi-unit activity from an animal expressing archaerhodopsin ('Arch'; ***p<0.0001, Wilcoxon signed rank test; d=1.42; 32 trials, 8 days, 5 animals). **c**. Normalized SWA before (low $[Cl^-]_i$) and after

(high $[Cl^-]_i$) halorhodopsin activation (5 s time bins) shows recovery kinetics following Cl^- loading (39 trials, 14 days, 5 animals). **d**. Normalized spike rate before and after halorhodopsin activation (5 s time bins) shows recovery kinetics following Cl^- loading (26 trials, 11 days, 5 animals). **e**. Normalized SWA before (low $[Cl^-]_i$) and after ('Arch control') archaerhodopsin activation (34 trials, 10 days, 5 animals). **f**. Normalized spike rate before and after archaerhodopsin activation (26 trials, 8 days, 5 animals). **g**. Representative LFP trace (0.5-12 Hz band pass filtered) during NREM sleep, recorded before (low $[Cl^-]_i$; top) and after (high $[Cl^-]_i$; bottom) halorhodopsin activation. Spikes are marked with dots. **h**. Spikes plotted on the Hilbert-transform of the filtered LFP signal. The OFF period was defined as the upward phase (30-150° angle) of high-amplitude SWA waveforms (>30% of baseline). **i**. Spike rate during the OFF phase of SWA was reduced after halorhodopsin activation (*p=0.0178, one sample t-test; t=2.538; df=25; d=0.5; 26 trials, 13 days, 5 animals). **j**. No change in spike rate after the Arch control (p=0.6238, one sample t-test; t=0.496; df=29; d=0.09; 30 trials, 8 days, 5 animals). **k**. Normalized spike rate (ON/OFF) during SWA was higher after halorhodopsin activation (***p<0.0001, Wilcoxon matched-pairs signed rank test; d=0.6; 25 trials, 11 days, 5 animals). **l**. No change in normalized spike rate (ON/OFF) during SWA recorded after the Arch control (p=0.948, Wilcoxon matched-pairs signed-ranks test; d=0.01; 29 trials, 8 days, 5 animals). Data represent mean ± sem. All tests are two sided.

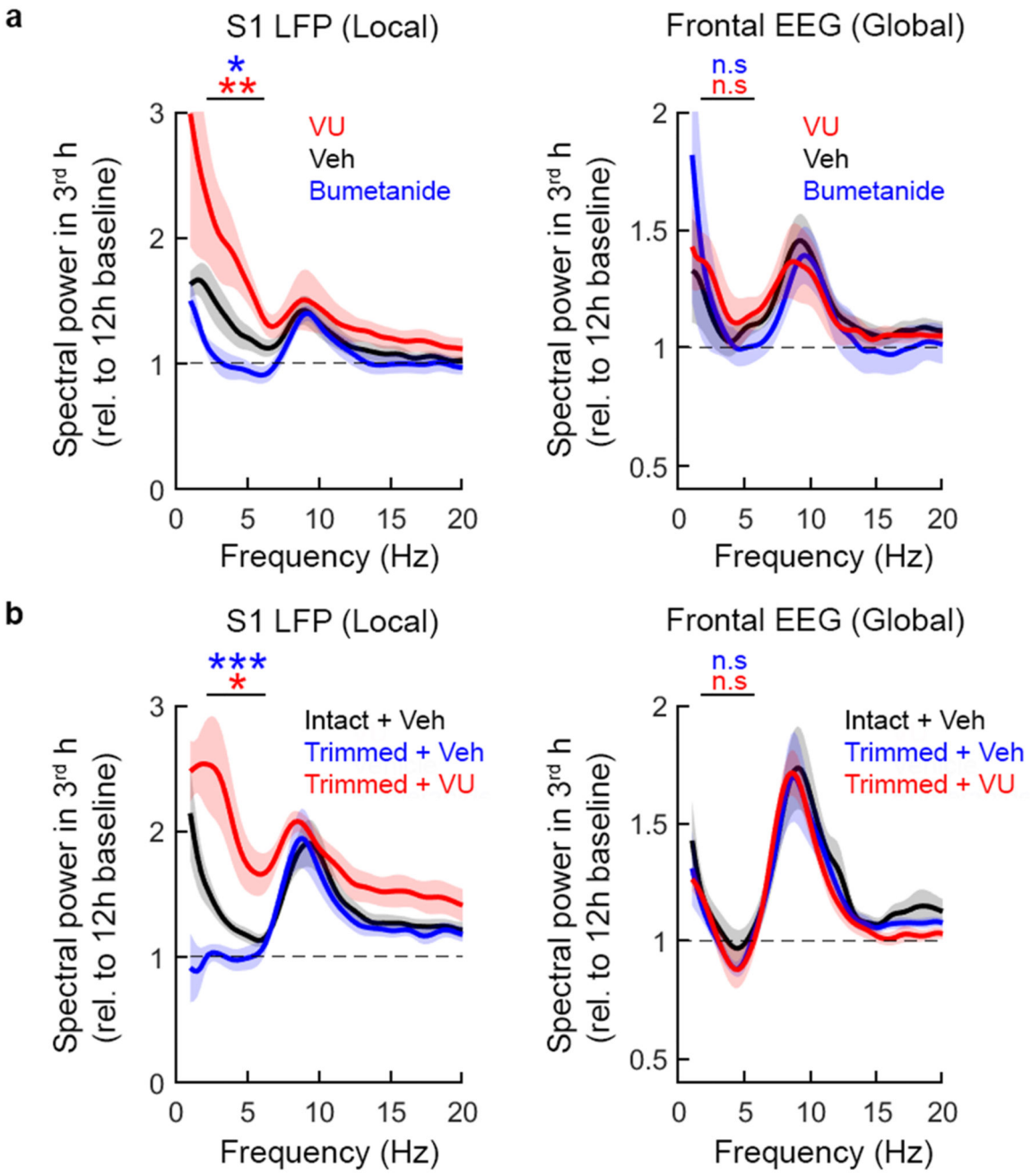

Extended Data Fig. 8.

$[Cl^-]_i$ regulation underlies local low-frequency cortical oscillations in the sleep-deprived awake state. Data from Fig. 6 is replotted by normalizing the LFP and EEG spectral power in the 3rd hour of the sleep-deprived awake state, to the preceding 12h baseline. Continuous awake LFP and EEG recordings were used to monitor local and global spectral power, respectively. Mice experienced a 3-hour SD protocol at the beginning of the light period (ZT0 to ZT3), during which $[Cl^-]_i$ was manipulated by locally infusing blockers of NKCC1 or KCC2 into S1. **a**. The awake LFP normalized to 12h baseline (left) revealed an increase in

low-frequency cortical oscillations (2-6Hz; black: 15 animals). The level of low-frequency oscillations was reduced by local infusion of bumetanide (blue versus black, *p=0.0116, paired t-test; t=3.582; df=6; d=1.35; blue: 7 animals, black: 7 animals) and increased by VU (red versus black, **p=0.0078, Wilcoxon matched-pairs signed-ranks test; d=0.89; red: 8 animals, black: 8 animals,). These manipulations did not affect the frontal EEG (right; blue versus black, p=0.5122, paired t-test; t=0.6965; df=6; d=0.26; blue: 7 animals, black: 7 animals; red versus black, p=0.4467, paired t-test; t=0.8255; df=5; d=0.34; red: 6 animals, black: 6 animals). **b**. To test the relationship of the low-frequency oscillations to activity-dependent processes during SD, whiskers were trimmed unilaterally just before the animal experienced the 3-hour SD protocol. Either vehicle control (Veh) or VU was infused unilaterally during SD. The awake LFP normalized to 12h baseline (left) revealed that whisker trimming prevented the increase in local low-frequency cortical oscillations (blue versus black, ***p=0.0007, paired t-test; t=6.452; df=6; d=2.44; blue: 7 animals, black: 7 animals). This effect could be rescued by VU infusion into S1 (red versus blue, *p=0.0122, unpaired t-test with Welch correction; t=3.541; df=6; d=1.4; red: 7 animals). Neither whisker trimming nor S1 infusion affected the increase in low-frequency oscillations detected in the frontal EEG (right; blue versus black, p=0.0873, paired t-test; t=2.041; df=6; d=0.77; red versus blue p=0.6495, unpaired t-test; t=0.47; df=12; d=0.9). Data represent mean ± sem. All tests are two sided.

Europe PMC Funders Author Manuscripts

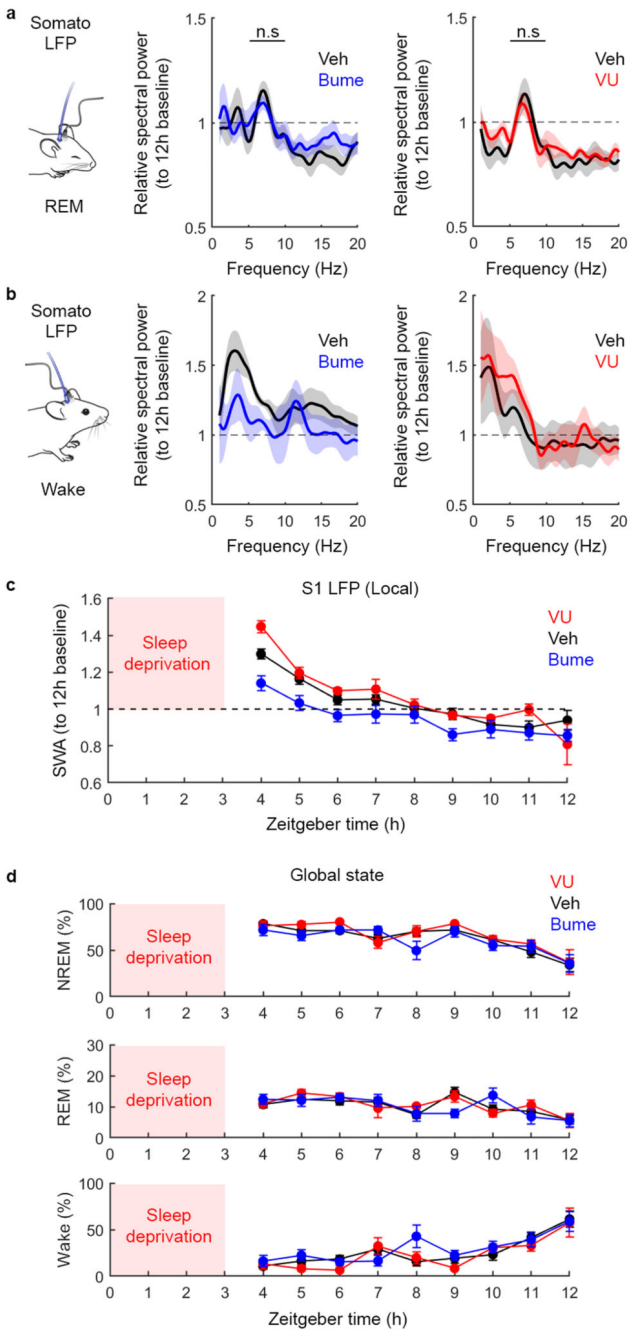

Extended Data Fig. 9.

Spectral power during different vigilance states after SD, time course of local NREM SWA after SD, and time course of vigilance state distribution after SD. Mice experienced a 3-hour SD protocol at the beginning of the light period (ZT0 to ZT3), during which $[Cl^-]_i$ was manipulated by locally infusing blockers of NKCC1 or KCC2 into S1. **a-b**. LFP spectral power during REM sleep ('a') and wake ('b') after SD. No differences were observed in theta frequency (5-10 Hz) during REM sleep with either bumetanide (left; p=0.985, paired t-test; t=0.02; df=5; d=0.01; black and blue: 6 trials, 5 animals) or VU (right; p=0.5625,

Wilcoxon matched-pairs signed-ranks test; d=0.4; black and red: 6 trials, 4 animals). In addition, when we compared ZT3 and ZT3-SD vehicle control animals, there was also no difference in theta frequency during REM (p=0.233, unpaired t-test; t=1.23; df=18; d=0.55). **c**. Time course of NREM SWA after SD, as derived from the S1 LFP (black: 12 trials, 9 animals; blue: 6 trials, 5 animals; red: 6 trials, 4 animals). **d**. Time course of vigilance states (i.e. global state) showing the proportion of time spent in NREM sleep (top), REM sleep (middle), and wake (bottom) after SD (black: 10 trials, 9 animals; blue: 5 trials, 5 animals, red: 5 trials, 4 animals). Data represent mean ± sem. All tests are two sided.

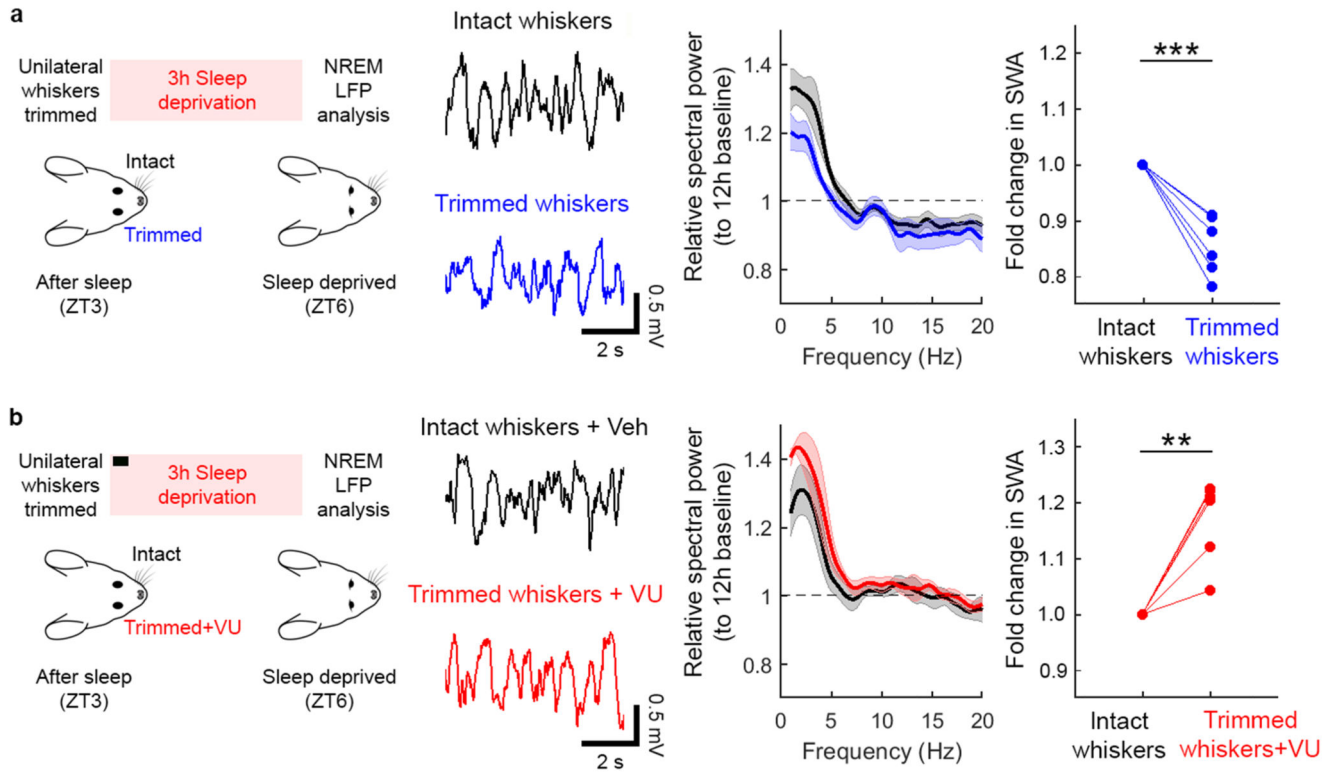

Extended Data Fig. 10. Activity-dependent regulation of cortical $[Cl^-]_i$ determines the high levels of local NREM SWA associated with sleep deprivation.

a. Whiskers were trimmed unilaterally at ZT3, when $[Cl^-]_i$ is normally low, and mice were then subjected to 3 hours of SD (left). NREM SWA was then analysed during the first 2 hours of sleep following SD. Example LFP signals (middle) show SWA recorded from S1 contralateral to intact whiskers ('intact'; black) and S1 contralateral to the trimmed whiskers ('trimmed'; blue). Data was collected from the same animal, with an interval of at least 2 days. The S1 contralateral to trimmed whiskers showed reduced SWA during NREM sleep (right; ***p=0.0004, one sample t-test; t=8.506; df=5; d=3.47; 6 animals). **b**. Using the same paradigm, $[Cl^-]_i$ was raised in S1 contralateral to the trimmed whiskers by local infusion of the KCC2 blocker, VU (horizontal bar indicates period of infusion). Other conventions as in 'a'. Pharmacologically raising $[Cl^-]_i$ reversed the reduction in SWA associated with whisker trimming (right; **p=0.0025, one sample t-test; t=5.583; df=5; d=2.28; 6 animals). Data represent mean ± sem. All tests are two sided.

Europe PMC Funders Author Manuscripts

Supplementary Material

Refer to Web version on PubMed Central for supplementary material.

Acknowledgments

We thank the Akerman lab for advice and comments, the Vyazovskiy Lab for support with *in vivo* electrophysiology experiments, Stuart Peirson and Aarti Jagannath for commenting on the manuscript. We thank Ethan Tyler, Lex Kravitz, Luigi Petrucco and Scidraw.io for providing the mouse drawings.

Funding

The research leading to these results received funding from a Sir Henry Wellcome Postdoctoral Fellowship 206500/Z/17/Z (HA), St John's College Junior Research Fellowship (HA), the European Research Council under grant agreement 617670 (CJA), MRC project MR/S01134X/1 and Wellcome Trust project 106174/Z/14/Z.

Data Availability

All relevant source data are provided with the manuscript. Example raw signals are included within the manuscript. Unprocessed electrophysiological recording data are available from the corresponding authors upon reasonable request.

Code availability

The code for automated vigilance scoring is available in open-source format at: https://github.com/paulbrodersen/somnotate[66]. The code for the neuronal network simulation is available in open-source format at: https://gist.github.com/paulbrodersen/b6ce791a927b7e7e714e6a322d90e2b7.

References

1. Vyazovskiy VV, et al. Local sleep in awake rats. Nature. 2011; 472: 443–447. [PubMed: 21525926]
2. Huber R, Ghilardi MF, Massimini M, Tononi G. Local sleep and learning. Nature. 2004; 430: 78–81. [PubMed: 15184907]
3. Nir Y, et al. Selective neuronal lapses precede human cognitive lapses following sleep deprivation. Nat Med. 2017; 23: 1474–1480. [PubMed: 29106402]
4. Tobler I, Borbély AA. Sleep EEG in the rat as a function of prior waking. Electroencephalogr Clin Neurophysiol. 1986; 64: 74–76. [PubMed: 2424723]
5. Wang Z, et al. Quantitative phosphoproteomic analysis of the molecular substrates of sleep need. Nature. 2018; 558: 435–439. [PubMed: 29899451]
6. Brüning F, et al. Sleep-wake cycles drive daily dynamics of synaptic phosphorylation. Science. 2019; 366
7. Ding F, et al. Changes in the composition of brain interstitial ions control the sleep-wake cycle. Science. 2016; 352: 550–555. [PubMed: 27126038]
8. Noya SB, et al. The forebrain synaptic transcriptome is organized by clocks but its proteome is driven by sleep. Science. 2019; 366
9. Vyazovskiy VV, et al. Cortical Firing and Sleep Homeostasis. Neuron. 2009; 63: 865–878. [PubMed: 19778514]
10. Huber R, Deboer T, Tobler I. Topography of EEG Dynamics After Sleep Deprivation in Mice. J Neurophysiol. 2000; 84: 1888–1893. [PubMed: 11024081]
11. Vyazovskiy VV, Welker E, Fritschy J-M, Tobler I. Regional pattern of metabolic activation is reflected in the sleep EEG after sleep deprivation combined with unilateral whisker stimulation in mice. Eur J Neurosci. 2004; 20: 1363–1370. [PubMed: 15341608]

12. Steriade M, Contreras D, Dossi RC, Nunez A. The slow (<1 Hz) oscillation in reticular thalamic and thalamocortical neurons: scenario of sleep rhythm generation in interacting thalamic and neocortical networks. J Neurosci. 1993; 13: 3284–3299. [PubMed: 8340808]
13. Thomas CW, Guillaumin MCC, McKillop LE, Achermann P, Vyazovskiy VV. Global sleep homeostasis reflects temporally and spatially integrated local cortical neuronal activity. Elife. 2020; 9: 1–25.
14. Kattler H, Dijk DJ, Borbely AA. Effect of unilateral somatosensory stimulation prior to sleep on the sleep EEG in humans. J Sleep Res. 1994; 3: 159–164. [PubMed: 10607121]
15. Siclari F, Tononi G. Local aspects of sleep and wakefulness. Current Opinion in Neurobiology. 2017; 44: 222–227. [PubMed: 28575720]
16. Diering GH, et al. Homer1a drives homeostatic scaling-down of excitatory synapses during sleep. Science. 2017; 355: 511–515. [PubMed: 28154077]
17. De Vivo L, et al. Ultrastructural evidence for synaptic scaling across the wake/sleep cycle. Science. 2017; 355: 507–510. [PubMed: 28154076]
18. Choi HJ, et al. Excitatory actions of GABA in the suprachiasmatic nucleus. J Neurosci. 2008; 28: 5450–5459. [PubMed: 18495878]
19. Wagner S, Castel M, Gainer H, Yarom Y. GABA in the mammalian suprachiasmatic nucleus and its role in diurnal rhythmicity. Nature. 1997; 387: 598–603. [PubMed: 9177347]
20. Raimondo JV, Markram H, Akerman CJ. Short-term ionic plasticity at GABAergic synapses. Front Synaptic Neurosci. 2012; 4
21. Düsterwald KM, et al. Biophysical models reveal the relative importance of transporter proteins and impermeant anions in chloride homeostasis. Elife. 2018; 7 39575
22. Kaila K, Price TJ, Payne JA, Puskarjov M, Voipio J. Cation-chloride cotransporters in neuronal development, plasticity and disease. Nat Rev Neurosci. 2014; 15: 637–654. [PubMed: 25234263]
23. Gulledge AT, Stuart GJ. Excitatory Actions of GABA in the Cortex. Neuron. 2003; 37: 299–309. [PubMed: 12546824]
24. Rivera C, et al. The K+/Cl- co-transporter KCC2 renders GABA hyperpolarizing during neuronal maturation. Nature. 1999; 397: 251–255. [PubMed: 9930699]
25. Pracucci E, et al. Circadian rhythm in cortical chloride homeostasis underpins variation in network excitability. bioRxiv. 2021; 2021.05.12.443725 doi: 10.1101/2021.05.12.443725
26. Fanselow EE, Connors BW. The roles of somatostatin-expressing (GIN) and fast-spiking inhibitory interneurons in up-down states of mouse neocortex. J Neurophysiol. 2010; 104: 596–606. [PubMed: 20538767]
27. Sanchez-Vives MV, et al. Inhibitory modulation of cortical up states. J Neurophysiol. 2010; 104: 1314–1324. [PubMed: 20554835]
28. Pouille F, Scanziani M. Enforcement of temporal fidelity in pyramidal cells by somatic feed-forward inhibition. Science. 2001; 293: 1159–1163. [PubMed: 11498596]
29. Alfonsa H, et al. The Contribution of Raised Intraneuronal Chloride to Epileptic Network Activity. J Neurosci. 2015; 35: 7715–7726. [PubMed: 25995461]
30. Raimondo JV, Kay L, Ellender TJ, Akerman CJ. Optogenetic silencing strategies differ in their effects on inhibitory synaptic transmission. Nat Neurosci. 2012; 15: 1102–1104. [PubMed: 22729174]
31. Finelli LA, Baumann H, Borbély AA, Achermann P. Dual electroencephalogram markers of human sleep homeostasis: Correlation between theta activity in waking and slow-wave activity in sleep. Neuroscience. 2000; 101: 523–529. [PubMed: 11113301]
32. Palchykova S, Winsky-Sommerer R, Meerlo P, Dürr R, Tobler I. Sleep deprivation impairs object recognition in mice. Neurobiol Learn Mem. 2006; 85: 263–271. [PubMed: 16423541]
33. Halassa MM, et al. Astrocytic Modulation of Sleep Homeostasis and Cognitive Consequences of Sleep Loss. Neuron. 2009; 61: 213–219. [PubMed: 19186164]
34. Warburton EC, Brown MW. Neural circuitry for rat recognition memory. Behav Brain Res. 2015; 285: 131–139. [PubMed: 25315129]
35. Wu H-PP, Ioffe JC, Iverson MM, Boon JM, Dyck RH. Novel, whisker-dependent texture discrimination task for mice. Behav Brain Res. 2013; 237: 238–242. [PubMed: 23026377]

36. Krueger JM, Nguyen JT, Dykstra-Aiello CJ, Taishi P. Local sleep. Sleep Med Rev. 2019; 43: 14–21. [PubMed: 30502497]
37. Nollet M, Wisden W, Franks NP. Sleep deprivation and stress: a reciprocal relationship. Interface Focus. 2020; 10 20190092 [PubMed: 32382403]
38. Milinski L, et al. Waking experience modulates sleep need in mice. BMC Biol. 2021; 19: 65. [PubMed: 33823872]
39. Havekes R, Aton SJ. Impacts of Sleep Loss versus Waking Experience on Brain Plasticity: Parallel or Orthogonal? Trends Neurosci. 2020; 43: 385–393. [PubMed: 32459991]
40. Doyon N, Vinay L, Prescott SA, De Koninck Y. Chloride Regulation: A Dynamic Equilibrium Crucial for Synaptic Inhibition. Neuron. 2016; 89: 1157–1172. [PubMed: 26985723]
41. Rainnie DG, Grunze HCR, McCarley RW, Greene RW. Adenosine inhibition of mesopontine cholinergic neurons: Implications for EEG arousal. Science. 1994; 263: 689–692. [PubMed: 8303279]
42. Watanabe M, Fukuda A. Development and regulation of chloride homeostasis in the central nervous system. Frontiers in Cellular Neuroscience. 2015; 9
43. Krone LB, et al. A role for the cortex in sleep–wake regulation. Nat Neurosci. 2021; 24: 1210–1215. [PubMed: 34341585]
44. Krueger JM, et al. Sleep as a fundamental property of neuronal assemblies. Nature Reviews Neuroscience. 2008; 9: 910–919. [PubMed: 18985047]
45. Tatsuki F, et al. Involvement of Ca2+-Dependent Hyperpolarization in Sleep Duration in Mammals. Neuron. 2016; 90: 70–85. [PubMed: 26996081]
46. Muheim CM, et al. Dynamic- and Frequency-Specific Regulation of Sleep Oscillations by Cortical Potassium Channels. Curr Biol. 2019; 29: 2983–2992. e3 [PubMed: 31474531]
47. Chauvette S, Seigneur J, Timofeev I. Sleep Oscillations in the Thalamocortical System Induce Long-Term Neuronal Plasticity. Neuron. 2012; 75: 1105–1113. [PubMed: 22998877]
48. Tononi G, Cirelli C. Sleep and synaptic homeostasis: A hypothesis. Brain Res Bull. 2003; 62: 143–150. [PubMed: 14638388]
49. Klinzing JG, Niethard N, Born J. Mechanisms of systems memory consolidation during sleep. Nature Neuroscience. 2019; 22: 1598–1610. [PubMed: 31451802]
50. Ferando I, Faas GC, Mody I. Diminished KCC2 confounds synapse specificity of LTP during senescence. Nat Neurosci. 2016; 19: 1197–1200. [PubMed: 27500406]
51. Meredith RM, Floyer-Lea AM, Paulsen O. Maturation of Long-Term Potentiation Induction Rules in Rodent Hippocampus: Role of GABAergic Inhibition. J Neurosci. 2003; 23: 11142–11146. [PubMed: 14657173]
52. Rijo-Ferreira F, Takahashi JS. Genomics of circadian rhythms in health and disease. Genome Med. 2019; 11: 82. [PubMed: 31847894]
53. Bae K, et al. Differential Functions of mPer1, mPer2, and mPer3 in the SCN Circadian Clock. Neuron. 2001; 30: 525–536. [PubMed: 11395012]
54. Deidda G, Bozarth IF, Cancedda L. Modulation of GABAergic transmission in development and neurodevelopmental disorders: investigating physiology and pathology to gain therapeutic perspectives. Front Cell Neurosci. 2014; 8: 119. [PubMed: 24904277]
55. Tang X, Jaenisch R, Sur M. The role of GABAergic signalling in neurodevelopmental disorders. Nature Reviews Neuroscience. 2021; 22: 290–307. [PubMed: 33772226]
56. Kyrozis A, Reichling DB. Perforated-patch recording with gramicidin avoids artifactual changes in intracellular chloride concentration. J Neurosci Methods. 1995; 57: 27–35. [PubMed: 7540702]
57. Katz Y, Yizhar O, Staiger J, Lampl I. Optopatcher—An electrode holder for simultaneous intracellular patch-clamp recording and optical manipulation. J Neurosci Methods. 2013; 214: 113–117. [PubMed: 23370312]
58. Ellender TJ, et al. Embryonic progenitor pools generate diversity in fine-scale excitatory cortical subnetworks. Nat Commun. 2019; 10 5224 [PubMed: 31745093]
59. Hansson-Sandsten M. Optimal multitaper wigner spectrum estimation of a class of locally stationary processes using Hermite functions. EURASIP J Adv Signal Process. 2011; 2011: 15.

60. Pedregosa F, et al. Scikit-learn: Machine learning in Python. J Mach Learn Res. 2011; 12: 2825–2830.
61. Schreiber J, Allen PG. pomegranate: Fast and Flexible Probabilistic Modeling in Python. Journal of Machine Learning Research. 2018; 18
62. McKillop LE, et al. Effects of aging on cortical neural dynamics and local sleep homeostasis in mice. J Neurosci. 2018; 38: 3911–3928. [PubMed: 29581380]
63. Sivakumaran S, et al. Selective Inhibition of KCC2 Leads to Hyperexcitability and Epileptiform Discharges in Hippocampal Slices and In Vivo. J Neurosci. 2015; 35: 8291–8296. [PubMed: 26019342]
64. Stimberg M, Brette R, Goodman DFM. Brian 2, an intuitive and efficient neural simulator. Elife. 2019; 8
65. Vogels TP, Sprekeler H, Zenke F, Clopath C, Gerstner W. Inhibitory plasticity balances excitation and inhibition in sensory pathways and memory networks. Science. 2011; 334: 1569–1573. [PubMed: 22075724]
66. Brodersen PJN, et al. Somnotate: An accurate, robust, and flexible sleep stage classifier for the experimentalist. bioRxiv. 2022; doi: 10.1101/2021.10.06.463356

Europe PMC Funders Author Manuscripts

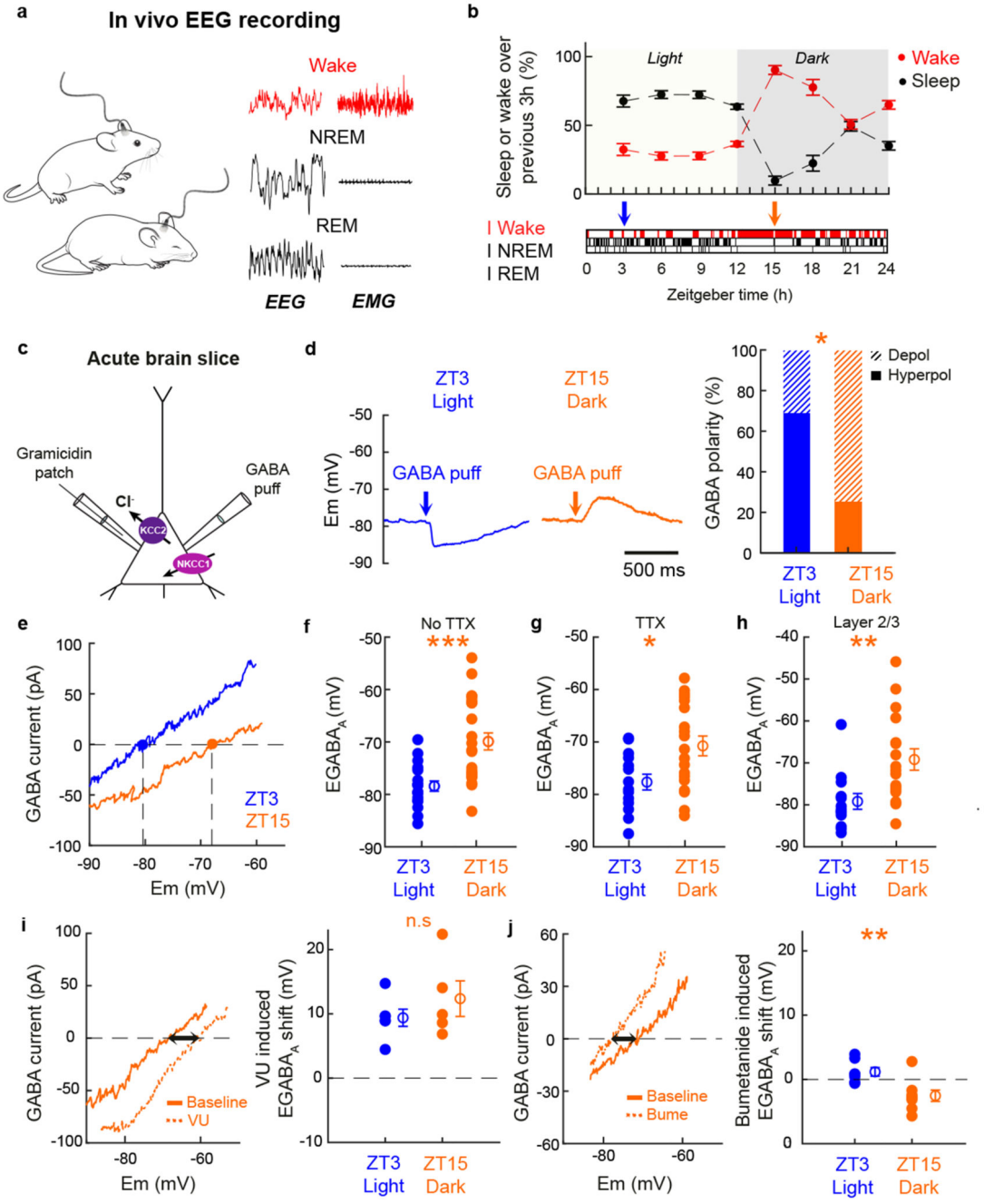

Fig. 1. Cortical pyramidal neurons exhibit diurnal variations in $EGABA_A$.

a. Continuous EEG and EMG recordings were performed in freely moving mice (left) and are shown during wake, NREM sleep and REM sleep (right). **b**. Time spent asleep or awake over 3-hour intervals (top; 10 x 24h recordings from 6 animals). Hypnogram shows typical distribution of vigilance states and arrows indicate when brain slices were prepared (bottom). **c**. Gramicidin perforated patch recordings examined $GABA_AR$ signalling in L5 pyramidal neurons of S1. **d**. Current clamp recordings show $GABA_AR$ responses in a slice prepared at ZT3 or at ZT15 (left). Proportion of depolarizing $GABA_AR$ responses (right)

was greater at ZT15 compared to ZT3 (*p=0.01, Fisher's exact test; blue: 19 neurons, 19 slices, 8 animals; orange: 20 neurons, 20 slices, 8 animals). **e**. $GABA_AR$ IV curves from a neuron at ZT3 or ZT15. $EGABA_A$ is the membrane potential at which the $GABA_AR$ current equals zero. **f**. $EGABA_A$ was more depolarized at ZT15 compared to ZT3 (***p=0.0003, Mann-Whitney test; d=1.29; blue: 18 neurons, 18 slices, 8 animals; orange: 24 neurons, 8 animals). **g**. A similar $EGABA_A$ difference was observed when action potential activity was blocked during recordings (*p=0.0109, unpaired t-test; t=2.708; df=31; d=0.95; blue: 14 neurons, 14 slices, 7 animals; orange: 19 neurons, 19 slices, 7 animals). **h**. A similar $EGABA_A$ difference was observed in L2/3 of auditory cortex (**p=0.006, unpaired t-test; t=2.97; df=28; d=1.09; blue: 13 neurons, 13 slices, 7 animals; orange: 17 neurons, 17 slices, 7 animals). **i**. The KCC2 cotransporter antagonist, VU0463271 ('VU'), induced a positive $EGABA_A$ shift at ZT15 (left). No significant difference was observed in the VU-induced $EGABA_A$ shift at ZT3 and ZT15 (right; p=0.332, unpaired t-test; t=1.025; df=9; d=0.62; blue: 6 neurons, 6 slices, 2 animals; orange: 5 neurons, 5 slices, 2 animals). **j**. The NKCC1 cotransporter antagonist, bumetanide ('Bume'), induced a negative $EGABA_A$ shift at ZT15 (left). Bumetanide induced larger $EGABA_A$ shifts at ZT15 than ZT3 (right; **p=0.0033, unpaired t-test; t=3.538; df=14; d=1.77; blue: 8 neurons, 8 slices, 5 animals; orange: 8 neurons, 8 slices, 4 animals). Data represent mean ± sem. All tests are two sided.

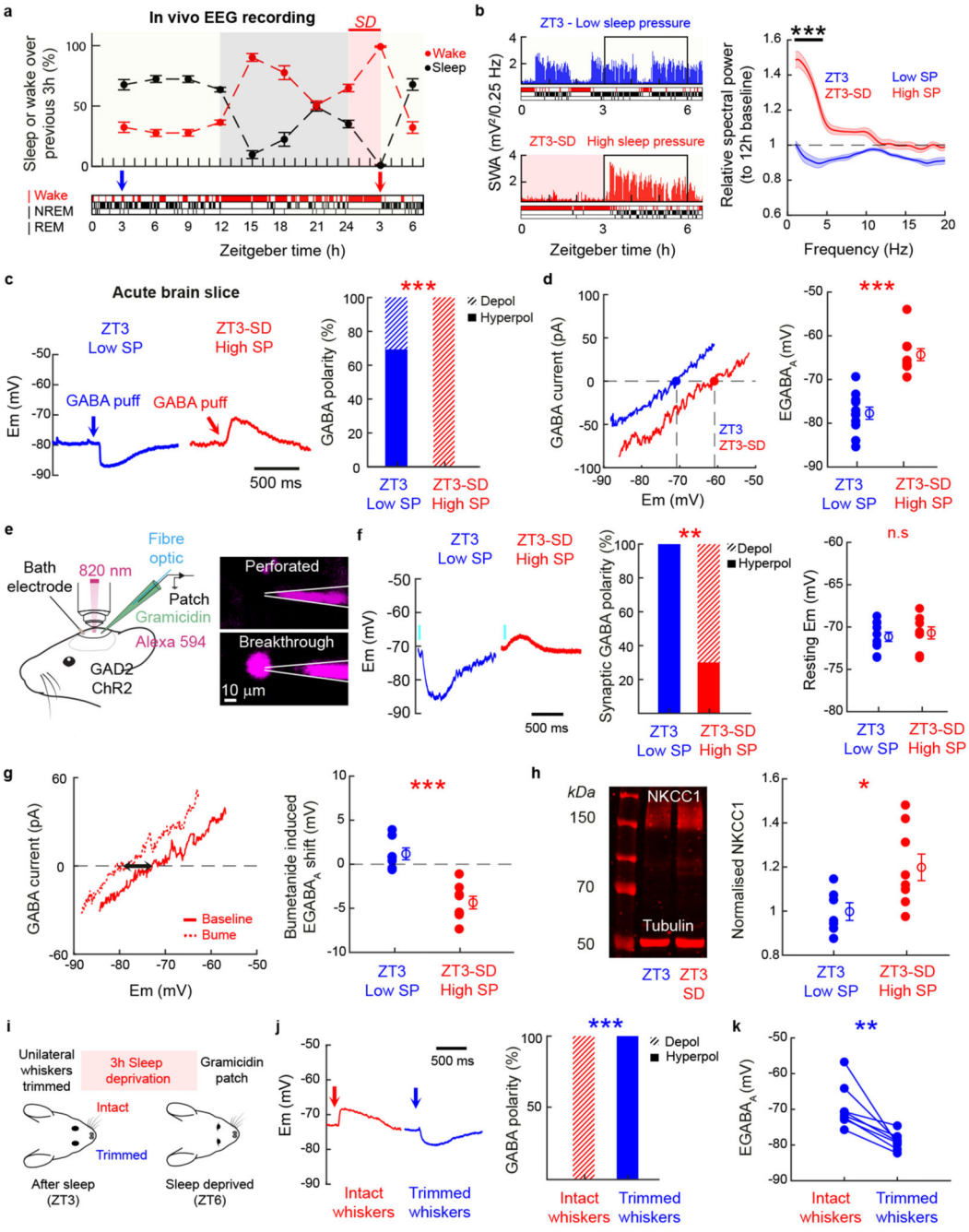

Fig. 2. Preceding sleep-wake history determines EGABA$_A$ in cortical pyramidal neurons.

a. Time spent asleep or awake under normal conditions and following a 3-hour sleep deprivation (SD) protocol performed at light onset (top; 5 days, 5 animals). Representative hypnogram (bottom), conventions as in Fig. 1. **b**. EEG SWA (left) recorded under normal conditions when sleep pressure (SP) was low (ZT3) or following the SD protocol when sleep pressure was high (ZT3-SD). Relative spectral power confirms high levels of NREM SWA in ZT3-SD (right; ***p<0001, paired t-test; t=11.642; df=9; d=3.68; 10 days, 6 animals; data from boxed EEG regions). **c**. Gramicidin current clamp recordings show the effect

Europe PMC Funders Author Manuscripts

of $GABA_AR$ activation upon a L5 pyramidal neuron from the ZT3 or ZT3-SD condition (left). Proportion of depolarizing $GABA_AR$ responses (right) was greater in ZT3-SD (***p<0.0001, Fisher's exact test; red: 10 neurons, 10 slices, 4 animals; blue: data from Fig. 1d). **d**. $GABA_AR$ IV curves from a neuron in the ZT3 or ZT3-SD condition (left). $EGABA_A$ (right) was more depolarized in ZT3-SD when sleep pressure was high (***p<0.0001, unpaired t-test; t=8.376; df=26; d=3.3; red: 10 neurons, 10 slices, 4 animals; blue: data from Fig. 1f). **e**. Gramicidin perforated patch recordings were performed in awake head-fixed mice expressing channelrhodopsin-2 (ChR2) in interneurons. **f**. Gramicidin current clamp recordings show effect of synaptic $GABA_AR$ activation upon a L2/3 pyramidal neuron in the ZT3 or ZT3-SD condition (left). Blue vertical lines indicate ChR2 activation. Proportion of depolarizing $GABA_AR$ responses (middle) was greater in the ZT3-SD condition (middle, **p=0.0065, Fisher's exact test; blue: 10 neurons, 7 animals; red: 8 neurons, 8 animals). No significant difference was observed in the resting membrane potential (right, p=0.65, unpaired t-test; t=0.46; df=16; d=0.25; blue: 10 neurons, 7 animals; red: 8 neurons, 8 animals). **g**. *In vitro* gramicidin recordings showed that bumetanide ('Bume') induced larger $EGABA_A$ shifts in the ZT3-SD condition than in the ZT3 condition (***p<0.0001, unpaired t-test; t=6.033; df=14; d=3.02; red: 8 neurons, 8 slices, 3 animals; blue: data from Fig. 1j). **h**. Western blot (left) comparing total NKCC1 levels in somatosensory cortex from a mouse in the ZT3 or ZT3-SD condition. Normalized NKCC1 levels (right) were increased in the ZT3-SD condition (*p=0.0193, unpaired t-test; t=2.668; df=13; d=1.38; blue: 7 animals; red: 8 animals). **i**. Whiskers were trimmed unilaterally at ZT3, when $EGABA_A$ is normally hyperpolarized, and mice were subjected to 3 hours of SD. **j**. Example gramicidin current clamp recordings (left) show the effect of $GABA_AR$ activation upon a L5 pyramidal neuron contralateral to the intact whiskers or contralateral to the trimmed whiskers, from the same animal. A higher proportion of hyperpolarizing $GABA_AR$ responses were observed contralateral to the trimmed whiskers (right; ***p<0.0005, Fisher's exact test; 8 pairs, 8 slices, 3 animals). **k**. $EGABA_A$ was more hyperpolarized in the hemisphere contralateral to the trimmed whiskers (**p=0.0078, Wilcoxon matched-pairs signed-ranks test; d=1.55; 8 pairs, 8 slices, 3 animals). Data represent mean ± sem. All tests are two sided.

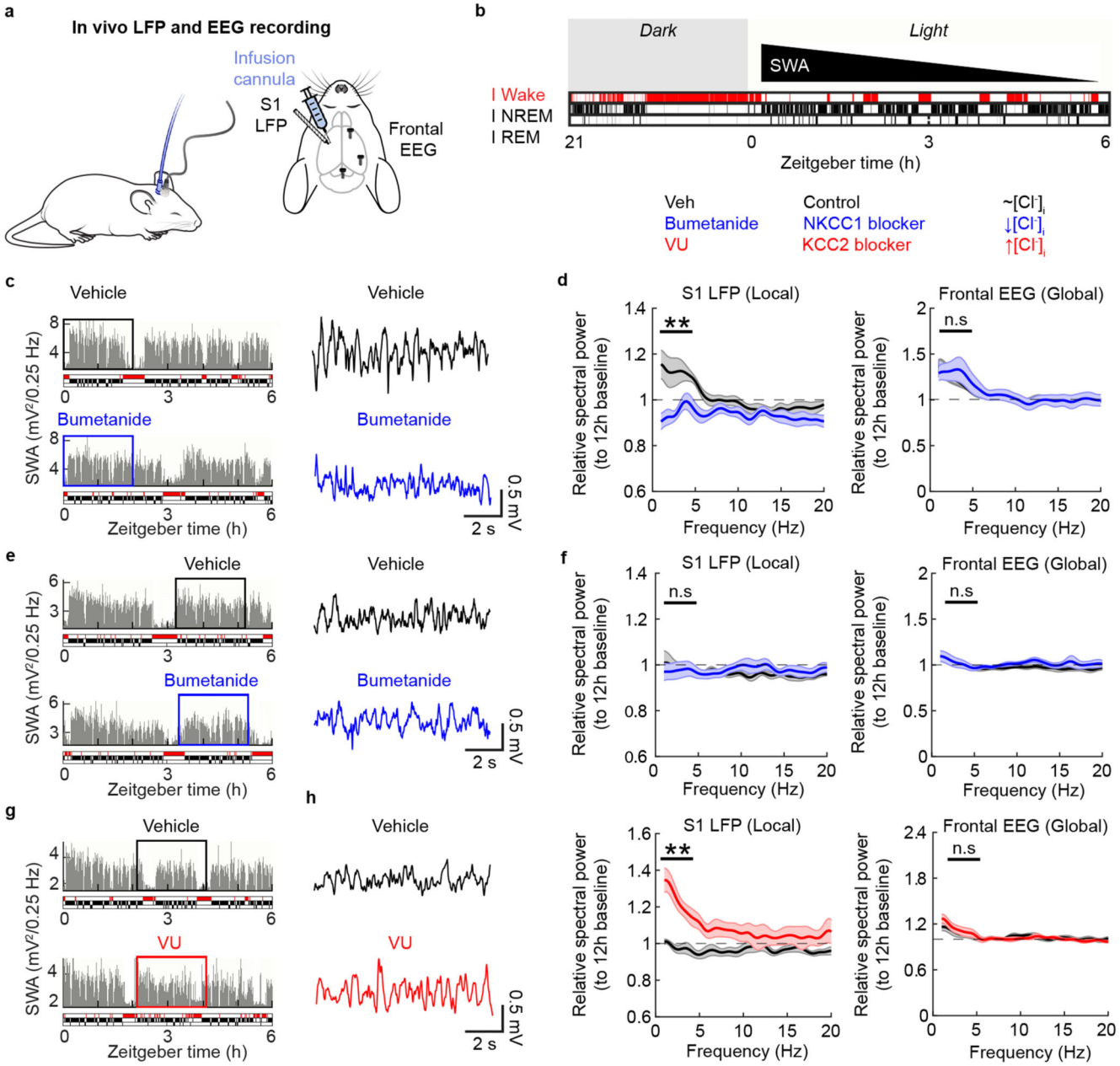

Fig. 3. Cortical $[Cl^-]_i$ regulation determines the level of local SWA during NREM sleep.

a. An LFP electrode coupled to an infusion cannula was targeted to L5 of left S1 and frontal EEG screws were positioned over the right hemisphere. Continuous LFP and EEG recordings were used to monitor local and global spectral power, respectively. **b.** SWA (black triangle) is most intense at sleep onset (coincident with light onset), when sleep pressure is high, and lessens over the course of sleep. $[Cl^-]_i$ was manipulated at different points during NREM sleep by locally infusing blockers of NKCC1 or KCC2. **c**. LFP in a mouse that received vehicle (top) or bumetanide (bottom) during early NREM sleep, on different days. Expanded traces (right) are from the boxed regions. **d**. Bumetanide infusion during early NREM sleep reduced local spectral power in the SWA range (left; **p=0.0027,

Europe PMC Funders Author Manuscripts

paired t-test; t=5.508; df=5; d=2.25; 6 trials, 5 animals), without affecting frontal EEG (right; p=0.3989, paired t-test; t=0.9219; df=5; d=0.38; 6 trials, 5 animals). **e**. LFP in a mouse that received either vehicle (top) or bumetanide (bottom) during later NREM sleep, when levels of SWA have reduced. **f**. Bumetanide infusion during later NREM sleep did not affect local spectral power in the SWA range (left; p=0.8006, paired t-test; t=0.2663; df=5; d=0.11; 6 trials, 5 animals), or frontal EEG (right; p=0.972, paired t-test; t=0.0368; df=5; d=0.01; 6 trials, 5 animals). **g**. LFP in a mouse that received infusion of vehicle (top) or VU (bottom) during later NREM sleep. **h**. VU infusion during later NREM sleep increased local spectral power in the SWA range (left; **p=0.0073, paired t-test; t=4.366; df=5; d=1.78; 6 trials, 4 animals), without affecting frontal EEG (right; p=0.355, paired t-test; t=1.019; df=5; d=0.42; 6 trials, 4 animals). Data represent mean ± sem. All tests are two sided.

Europe PMC Funders Author Manuscripts

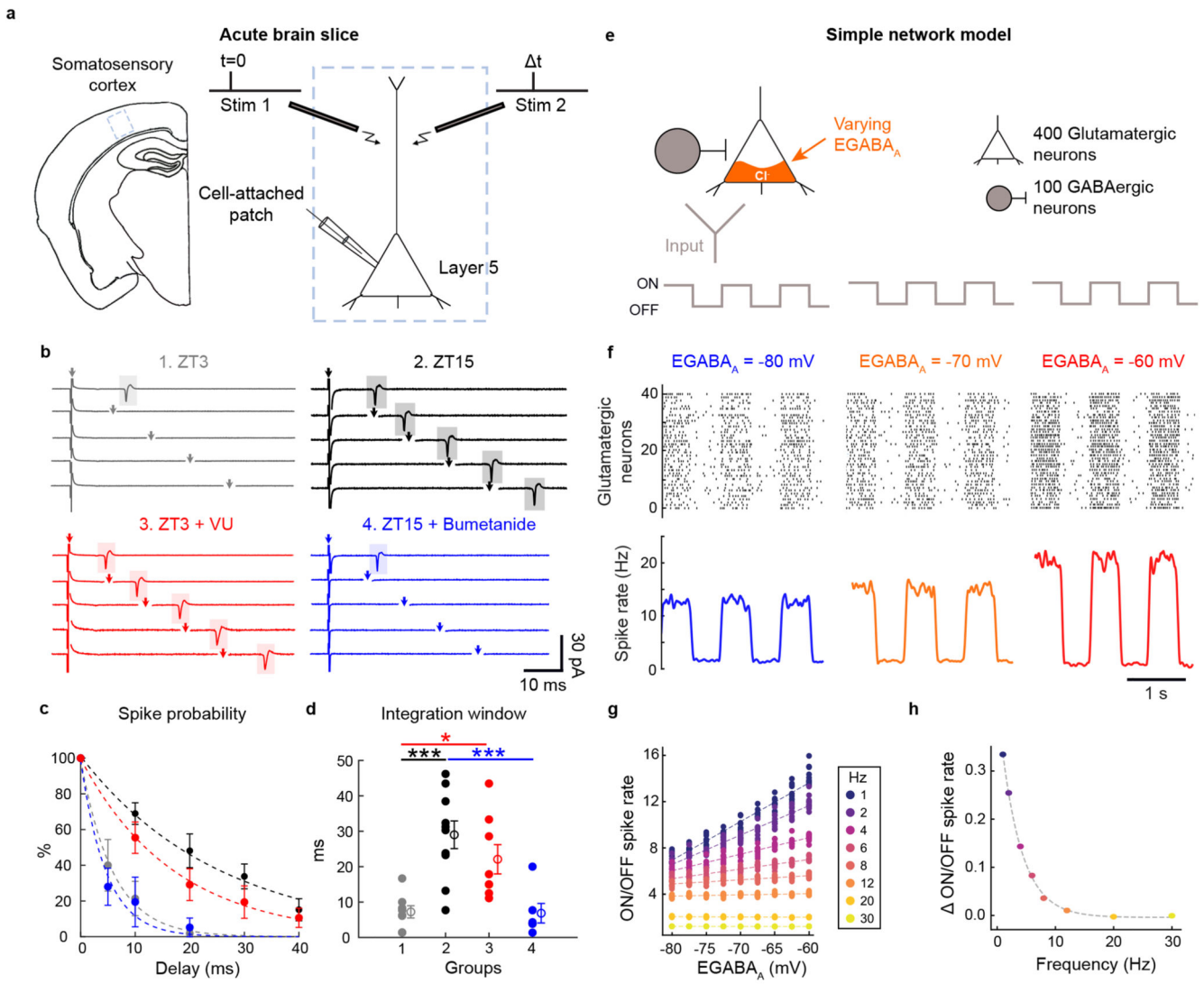

Fig. 4. Sleep-wake dependent EGABA$_A$ determines how easily a cortical neuron is recruited to spike.

a. Cell-attached recordings were used to measure the spiking probability of S1 L5 pyramidal neurons in response to the stimulation of two independent L2/3 input pathways, across different inter-stimulus delays. **b**. Spiking activity for different inter-stimulus delays in a neuron from the ZT3 low sleep pressure condition, the ZT15 higher sleep pressure condition, ZT3 in the presence of VU, or ZT15 in the presence of bumetanide. Downward vertical arrows indicate the time of the second stimulus and individual spikes are highlighted with shading. **c**. Normalized spike probability for different inter-stimulus delays and conditions (grey: 8 neurons, 8 slices, 3 animals; black: 10 neurons, 10 slices, 3 animals; red: 8 neurons, 8 slices, 2 animals; blue: 6 neurons, 6 slices, 2 animals) Color-coding as in 'b'. **d**. The synaptic integration window for spiking (defined as the time constant of spike probability data in 'c') for each of the experimental conditions. Color-coding as in 'b'. Integration windows are shorter at ZT3 compared to ZT15 (grey versus black; ***p<0.001, Tukey-Kramer post-test; q=6.575; d=2.22), are decreased following NKCC1 blockade at

ZT15 (blue versus black; ***p<0.001, Tukey-Kramer post-test; q=6.145; d=2.07), and increased following VU at ZT3 (red versus grey; *p<0.05, Tukey-Kramer post-test; q=4.26; d=1.66). Multiple groups comparison p<0.0001, one-way ANOVA. **e**. Simple network model to compare neuronal recruitment as a function of $[Cl^-]_i$ and therefore $EGABA_A$. The model comprised 400 glutamatergic neurons and 100 GABAergic neurons, each receiving synchronous oscillatory input to simulate ON and OFF periods. **f**. Raster plots of excitatory neuron spiking activity in response to a 1 Hz input, for three different $EGABA_A$ values. **g**. Depolarized $EGABA_A$ values are associated with greater neuronal recruitment during ON periods (spike rate normalized to OFF periods). **h**. $EGABA_A$ values affect neuronal recruitment for lower frequencies of oscillatory input. Data represent mean ± sem. All tests are two sided.

Europe PMC Funders Author Manuscripts

Europe PMC Funders Author Manuscripts

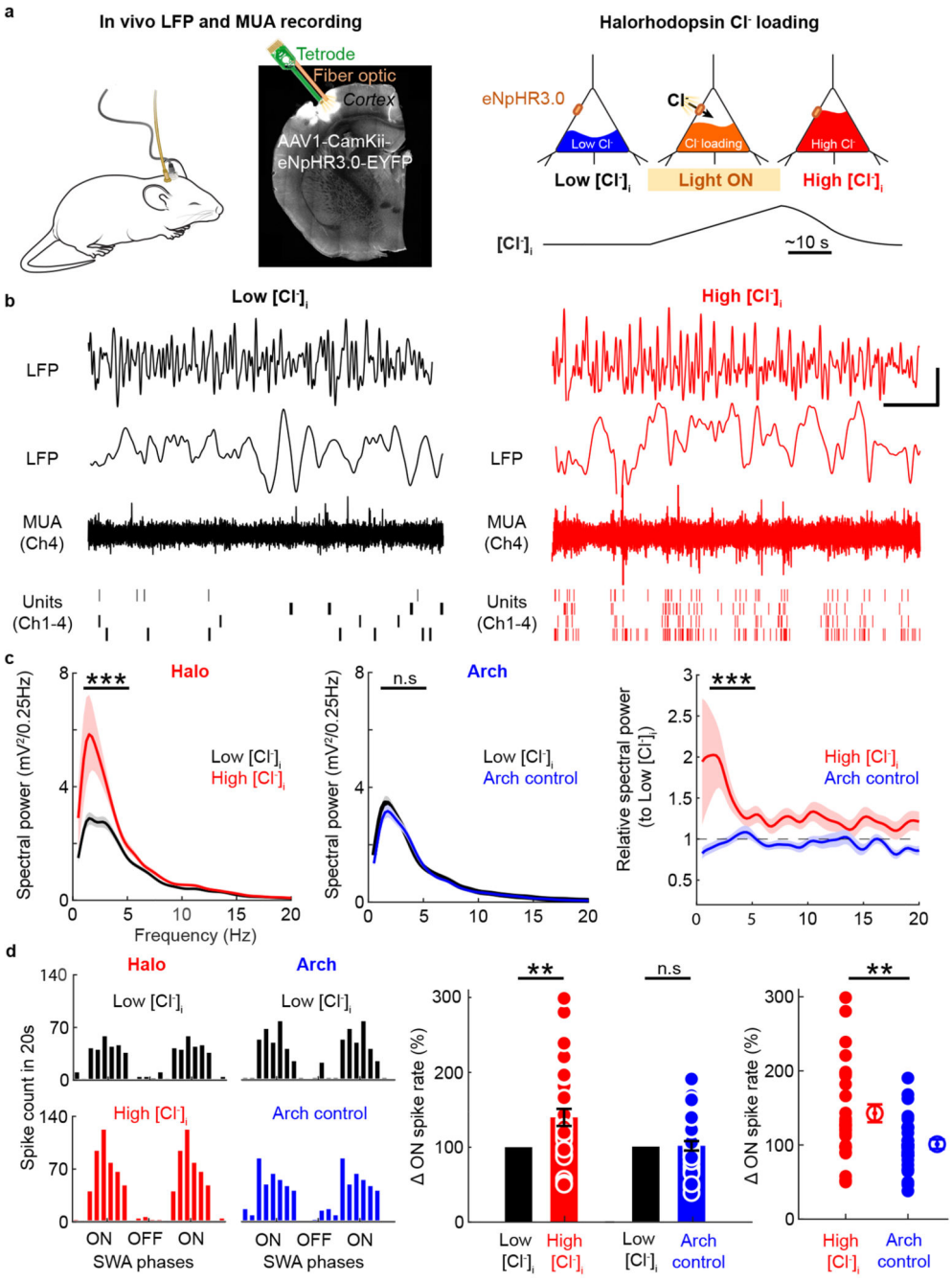

Fig. 5. Depolarized $EGABA_A$ boosts NREM SWA by enhancing cortical neuronal recruitment *in vivo*.

a. Halorhodopsin ('Halo', eNpHR3.0) was expressed in S1 excitatory cortical neurons and a combined tetrode and fibre optic implant were targeted to L5 *in vivo* (left). Optogenetic experiments were performed during periods of NREM sleep at ZT3, when sleep pressure is typically reduced and $EGABA_A$ is normally hyperpolarizing. The recordings compared 20 s epochs before light activation, when $[Cl^-]_i$ would be 'low', with 20 s epochs immediately after a period of Halo activation, when the opsin's effect on the membrane potential is over,

but $[Cl^-]_i$ would still be ‘high’ (right). **b**. LFP (top), expanded LFP (middle), and multi-unit spiking activity (bottom) under low $[Cl^-]_i$ (left) and high $[Cl^-]_i$ (right) conditions. Scale bar, x-axis is 2 s (LFP) and 230 ms (enlarged LFP, MUA and individual units) and y-axis is 0.5 mV (LFP and enlarged LFP) or 40 μV (MUA). Positivity is denoted as positive deflections of the signals. **c**. LFP spectral power in the SWA range increased after Halo activation (left; ***p<0.0001, Wilcoxon matched-pairs signed-ranks test; d=0.91; 38 trials, 14 days, 5 animals), but not after activation of archaerhodopsin (‘Arch’), which served as a control for membrane hyperpolarization (middle; p=0.094, Wilcoxon matched-pairs signed-ranks test; d=0.3; 34 trials, 10 days, 5 animals; right; ***p<0.0001, Mann-Whitney test; d=1.25). **d**. Representative phase-plots (left) of multi-unit spiking relative to SWA before (top) and after (bottom) activation of Halo or Arch. Halo-mediated Cl^- loading increased spike rate during ON periods of SWA (middle; red: **p=0.0022, Wilcoxon signed-ranks test; d=0.64, 30 trials, 13 days, 5 animals; blue: p=0.867, one sample t-test; t=0.169; df=29; d=0.03, 30 trials, 8 days, 5 animals; right; **p=0.0051, Mann-Whitney test; d=0.77). Data represent mean ± sem. All tests are two sided.

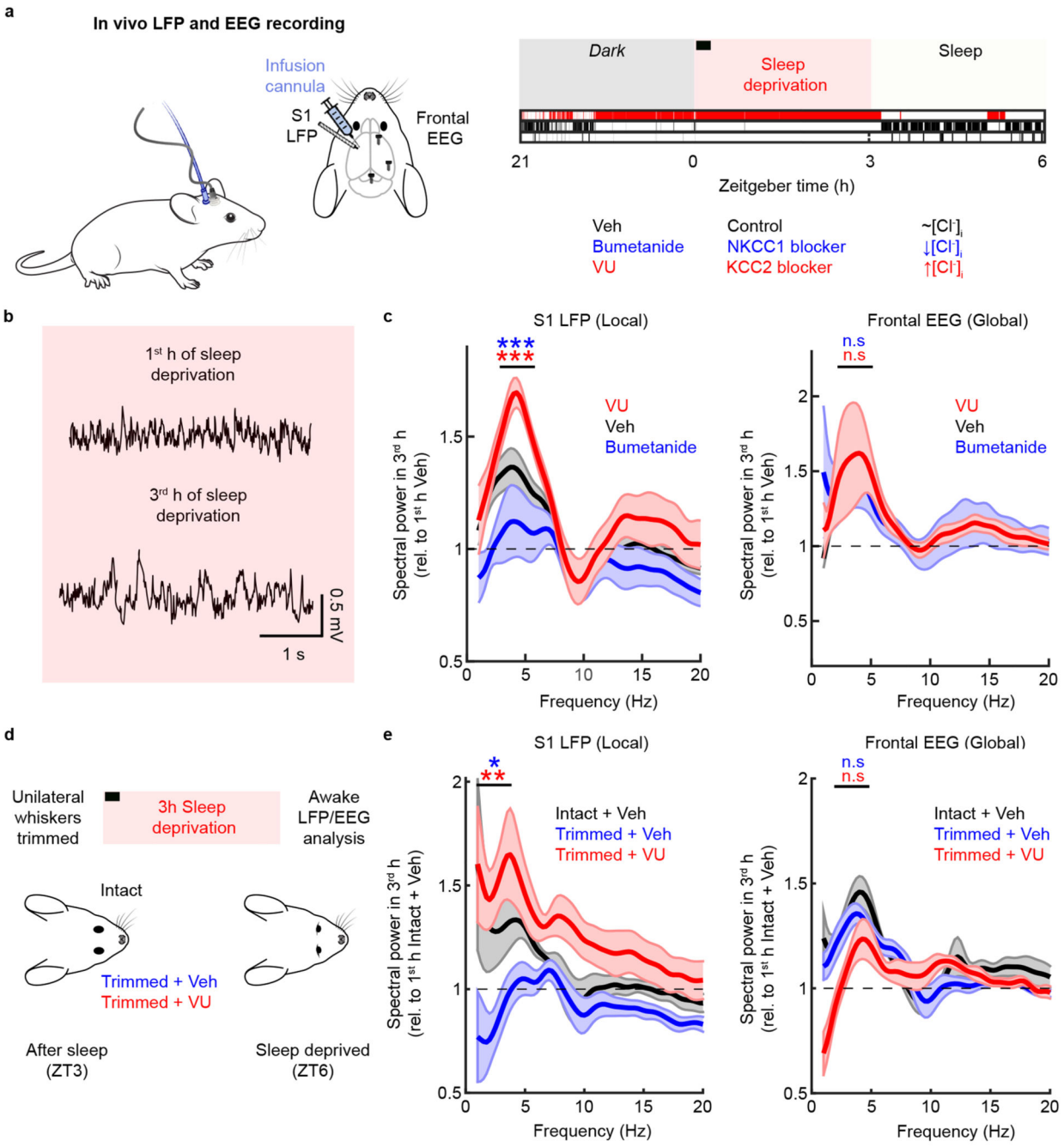

Fig. 6. $[Cl^-]_i$ regulation underlies local low-frequency cortical oscillations in the sleep-deprived awake state.

a. An LFP electrode and infusion cannula were targeted to L5 of left S1 and frontal EEG screws were positioned over the right hemisphere (left). Continuous awake LFP and EEG recordings were used to monitor local and global spectral power, respectively. Mice experienced a 3-hour SD protocol at the beginning of the light period (ZT0 to ZT3), during which $[Cl^-]_i$ was manipulated by locally infusing blockers of NKCC1 or KCC2 into S1 (right; horizontal bar). **b**. Awake LFP traces from a control mouse show increase

in low-frequency oscillations between the 1st hour (top) and 3rd hour (bottom) of SD. **c**. Awake LFP (left) revealed an increase in the level of low-frequency oscillations (2-6Hz; black: 15 animals), which was reduced by bumetanide (blue versus black, ***p<0.0001, paired t-test; t=10.636; df=6; d=4.02; blue: 7 animals, black: 7 animals) and increased by VU (red versus black, ***p=0.0078, Wilcoxon matched-pairs signed-ranks test; d=1.54; red: 8 animals, black: 8 animals). These manipulations did not affect the frontal EEG (right; blue versus black, p=0.9375, Wilcoxon matched-pairs signed-ranks test; d=0.12; red versus black, p=0.9304, paired t-test; t=0.0918; df=5; d=0.04). **d**. To test the relationship of the low-frequency oscillations to activity-dependent processes during SD, whiskers were trimmed unilaterally just before the animal experienced a 3-hour SD protocol. Vehicle control (veh) or VU was infused unilaterally during SD (horizontal bar indicates period of infusion). **e**. The awake LFP (left) revealed that whisker trimming prevented the increase in local low-frequency oscillations (blue versus black, *p=0.0167, paired t-test; t=3.284; df=6; d=1.24; blue: 7 animals, black: 7 animals). This effect could be rescued by VU infusion into S1 (red versus blue, **p=0.0032, unpaired t-test; t=3.679; df=12; d=1.97; red: 7 animals). Neither whisker trimming nor S1 infusion affected the increase in low-frequency oscillations detected in the frontal EEG (right; black versus blue, p=0.135, paired t-test; t=1.72; df=6; d=0.65; blue versus red, p=0.3592, unpaired t-test; t=0.9505; df=13; d=0.49). Data represent mean ± sem. All tests are two sided.

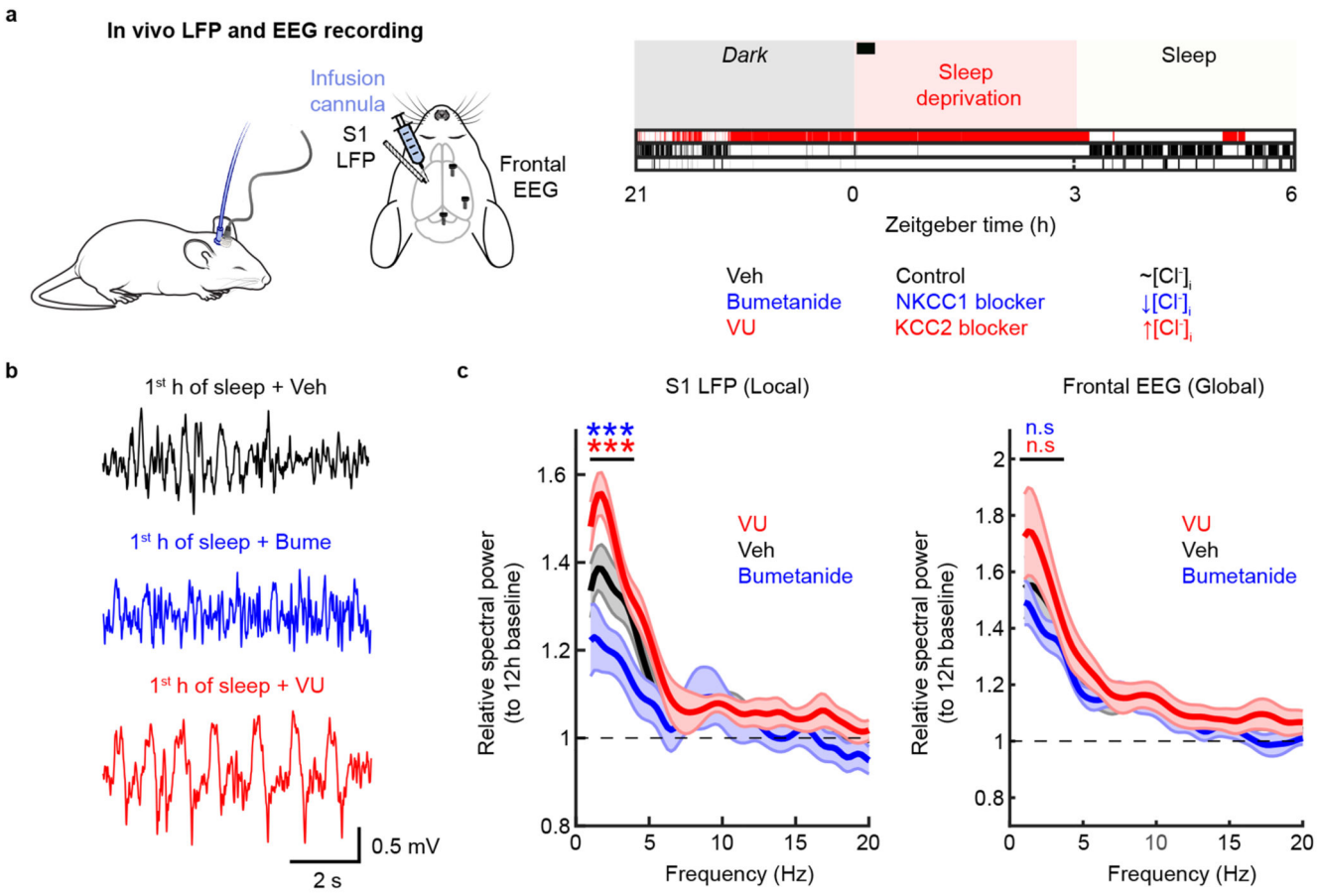

Fig. 7. $[Cl^-]_i$ regulation affects the levels of local NREM SWA observed with sleep deprivation.

a. Continuous S1 LFP and EEG recordings were used to monitor local and global spectral power, respectively, as mice entered NREM sleep following a 3-hour SD protocol at the beginning of the light period (ZT0 to ZT3). $[Cl^-]_i$ was manipulated by locally infusing blockers of NKCC1 or KCC2 into S1 (horizontal bar indicates period of infusion). **b**. LFP traces recorded during the 1st hour of NREM sleep immediately after SD, in a mouse receiving vehicle (top), bumetanide (middle) or VU (bottom) infusion. **c**. Bumetanide infusion reduced local spectral power in the SWA range during NREM sleep (left; blue versus black, ***p=0.0001, paired t-test; t=10.47; df=5; d=4.27; blue: 6 trials, 5 animals, black: 6 trials, 5 animals), while VU infusion increased local spectral power in the SWA range (red versus black, ***p=0.0007, paired t-test; t=7.5; df=5; d=3.06; red: 6 trials, 5 animals, black: 6 trials, 5 animals). There was no effect upon frontal EEG (right; blue versus black, p=0.611, paired t-test; t=0.54; df=5; d=0.22; red versus black, p=0.177, paired t-test; t=1.57; df=5; d=0.64). Data represent mean ± sem. All tests are two sided.

Europe PMC Funders Author Manuscripts

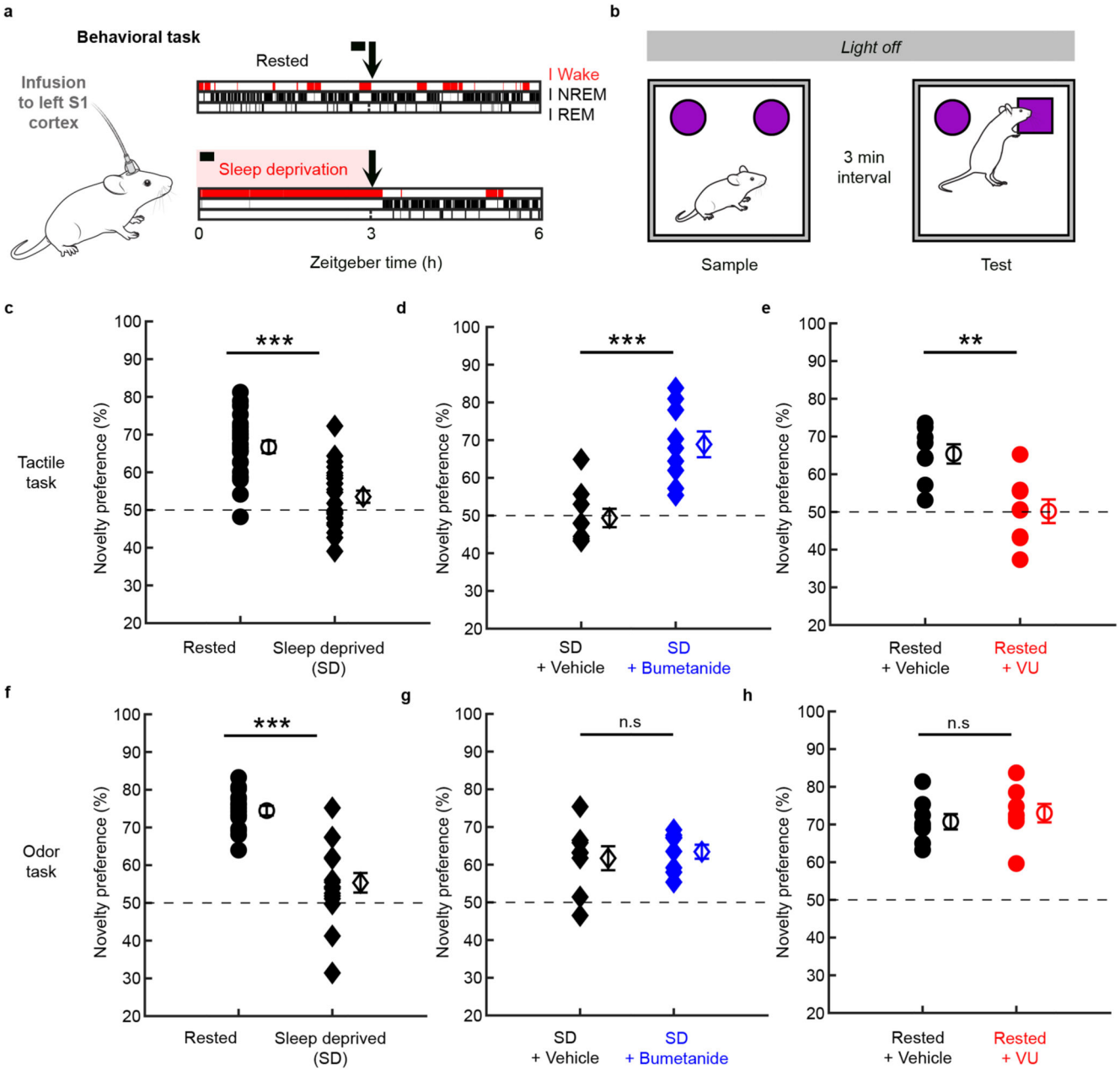

Fig. 8. Cortical $[Cl^-]_i$ regulation underlies performance levels in the sleep-deprived awake state.

a. Behavioral performance was tested at ZT3 in either 'rested' mice that had been allowed to sleep, or sleep-deprived ('SD') mice that had experienced a 3-hour SD protocol at the beginning of the light period. Blockers of NKCC1 or KCC2 were locally infused via a cannula targeted to left S1 (horizontal bars indicate period of infusion, arrows indicate time of behavioral task). **b**. A recognition memory paradigm tested novelty preference in the somatosensory modality ('tactile task'), as shown. In addition, an odor-based task ('odor task') served as a control for sensory modality that was remote from the infusion site (see Methods). Each behavioral trial began with a 'Sample' period, in which exploration time was yoked for total stimulus investigation time (60 s for the tactile task, 30 s for the

odor task). The animal was then returned to its home cage for a 3 minute interval, after which the animal began the 'Test' period. **c**. SD mice showed lower novelty preference on the tactile task (***p<0.0001, unpaired t-test; t=5.779; df=46; d=1.67; 24 trials, 12 animals). **d**. Bumetanide infusion into S1 increased tactile task novelty preference in SD mice (***p=0.0003, unpaired t-test; t=4.647; df=16; d=2.19; 9 trials, 9 animals). **e**. VU infusion into S1 decreased tactile task novelty preference in rested mice (**p=0.0021, unpaired t-test; t=3.76; df=14; d=1.88; 8 trials, 8 animals). **f**. SD mice showed lower novelty preference on the odor task (***p<0.0001, unpaired t-test; t=6.625; df=30; d=2.34; 16 trials, 8 animals). **g**. Bumetanide infusion into S1 did not affect odor task novelty preference in SD mice (p=0.6489, unpaired t-test; t=0.46; df=14; d=0.23; 8 trials, 8 animals). **h**. VU infusion into S1 did not affect odor task novelty preference in rested mice (p=0.4866, unpaired t-test; t=0.7146; df=14; d=0.36; 8 trials, 8 animals). Data represent mean ± sem. All tests are two sided.